

ZINC DIFFUSION IN GaAsSb FROM SPIN-ON GLASS DOPANT SOURCES

A Thesis

Submitted to the Graduate School
of the University of Notre Dame
in Partial Fulfillment of the Requirements
for the Degree of

Master of Science

by

Shishir K. Rai, B.Tech.

Patrick Fay, Director

Graduate Program in Electrical Engineering

Notre Dame, Indiana

December 2004

ZINC DIFFUSION IN GaAsSb FROM SPIN-ON GLASS DOPANT SOURCES

Abstract

by

Shishir K. Rai

The first study of p-type doping in GaAsSb lattice-matched to InP from Zn spin-on glass sources is reported. Shallow diffusion profiles suitable for aggressively-scaled heterojunction devices and good electronic transport properties in the doped films have been observed. Potential applications for spin-on doping of p-type GaAsSb include the optimization of the extrinsic base resistance and the contact resistance to the base in GaAsSb/InP HBTs for ultra-high-speed applications, without the use of regrowth or other complex processing.

Diffusions were carried out in a rapid thermal processor (RTP) using epitaxial heterostructures consisting of 2000 Å of p-type GaAs_{0.51}Sb_{0.49} grown on semi-insulating InP by MOCVD. The diffusions were performed at temperatures ranging from 350–625 °C and diffusion times of up to 30 minutes. SIMS depth profiling indicates that Zn starts to diffuse into GaAsSb layer at temperatures as low as 350 °C, forming very shallow diffusion profiles. For higher temperatures deep diffusion profiles extending up to 2500 Å were obtained. The Zn appears to remain largely electrically inactive for diffusions at temperatures below 500 °C, as indicated by Hall-effect measurements. The threshold temperature at which Zn starts to become electrically active is found to be in the range of 500–550 °C. Hall-effect measurements indicate that the average hole concentration increased by almost three

orders of magnitude for the lowest-doped ($2.05 \times 10^{16} \text{ cm}^{-3}$) test structure, rising from $2.05 \times 10^{16} \text{ cm}^{-3}$ to $1.67 \times 10^{19} \text{ cm}^{-3}$ for a 30 minute, 600 °C diffusion. The measured sheet resistance decreased from 280 k Ω /sq. to 910 Ω /sq., while the hole mobility was reduced from 59 cm²/Vs as-grown to 26 cm²/Vs due to increased impurity scattering. With increase in as-grown background doping concentration, the diffusion rate was found to increase.

Zn distribution profiles measured by SIMS were modeled and a mechanism for Zn diffusion in undoped GaAs_{0.51}Sb_{0.49} is proposed. Zn diffuses by an interstitial-substitutional mechanism in the region close to the surface but as it moves away from the surface and Zn concentration falls down, it diffuses by substitutional mechanism. Surface diffusivity of $1 \times 10^{-13} \text{ cm}^2/\text{s}$ at 600 °C for Zn interstitials is extracted from the diffusion profiles. Zn diffusivity away from the surface is found to be $1\text{--}2 \times 10^{-14} \text{ cm}^2/\text{s}$ at 600 °C. There is insufficient evidence to tell whether this diffusivity is that of substitutional Zn or of a complex that Zn atoms form with the surrounding defects.

CONTENTS

FIGURES	iv
TABLES	vi
ACKNOWLEDGMENTS	vii
CHAPTER 1: INTRODUCTION AND MOTIVATION	1
CHAPTER 2: EXPERIMENTAL PROCEDURE	7
2.1 Diffusion Experiments	7
2.1.1 Sample Preparation	8
2.1.2 Hall-effect Measurements	10
2.1.3 Error Analysis for Hall-effect Measurements	11
2.1.4 SIMS Analysis	13
2.2 TLM Experiments	14
2.2.1 Sample Preparation	15
2.2.2 TLM Measurements	17
CHAPTER 3: RESULTS AND DISCUSSION	18
3.1 Results of Diffusion Experiments	18
3.1.1 Hall-effect measurements	18
3.1.2 SIMS Profiles	22
3.1.3 Zinc Activation	27
3.2 Zinc Diffusion in 400 Å GaAsSb Base Layer for HBT Application	31
3.3 Results of TLM Measurements	35
CHAPTER 4: DIFFUSION MODELING	39
4.1 Diffusion in III-V Semiconductors [19]	39
4.2 Diffusion of Zn in GaAs [19]	41
4.3 Diffusion of Zn in GaSb	46
4.4 Diffusion of Zn in GaAsSb	50

CHAPTER 5: CONCLUSION 56

BIBLIOGRAPHY 58

FIGURES

1.1	Equilibrium band diagram for InP/GaAs _{0.51} Sb _{0.49} /InP DHBT.	3
1.2	Equilibrium band diagram for InP/In _{0.53} Ga _{0.47} As/InP DHBT.	3
1.3	(a) Cross section of a conventional HBT fabricated by mesa etch process. (b) Cross section of HBT showing additional dopants in the extrinsic base introduced by a spin-on dopant process.	5
2.1	Processing steps for Zn diffusion from spin-on glass films.	8
2.2	Typical temperature profile during rapid thermal diffusion.	10
2.3	Sample used for Hall-effect measurements showing the average diameter ‘d’ of the indium contacts and the dimension ‘L’ of its edge. The error in measurement due to finite size of the contact is of the order of ‘d/L’ [13].	12
3.1	Hole concentration with respect to Zn diffusion time for temperatures ranging from 500–600 °C for the structures 233 and 236 with different background doping.	19
3.2	Sheet resistance with respect to Zn diffusion time for temperatures ranging from 500–600 °C for the structures 233 and 236 with different background doping.	20
3.3	Mobility with respect to Zn diffusion time for temperatures ranging from 500–600 °C for the structures 233 and 236 with different background doping.	20
3.4	Zn profile for a 30 minute diffusion at temperatures ranging from 500–600 °C.	23
3.5	Zn distribution profiles in structure 236 for temperatures ranging from 500–600 °C.	23
3.6	Zn distribution profiles in structure 233 for temperatures 500 °C and 600 °C.	24
3.7	Plot showing the initial diffusion stage (IDS) and steady state Zn distribution (450 °C, 30 minute diffusion) profile in InP (Kamanin <i>et al.</i> [15]).	25

3.8	Plot showing Zn, In, As, Sb profiles in 2000 Å GaAsSb on InP. Zn diffusion was carried out at 600 °C for 30 minutes.	26
3.9	Zn activation in structures 233 and 236 with respect to the diffusion conditions.	30
3.10	SIMS distribution profile of Zn, Ga, As, Sb and P in 272-HBT GaAsSb base layer after a 600 °C, 30 s rapid thermal diffusion.	33
3.11	SIMS distribution profile of Zn, Ga, As, Sb and P in 272-HBT GaAsSb base layer after a 600 °C, 60 s rapid thermal diffusion.	33
3.12	SIMS distribution profile of Zn, Ga, As, Sb and P in 272-HBT GaAsSb base layer after a 625 °C, 30 s rapid thermal diffusion.	34
3.13	I-V curve for metal (Ti/Pt/Au) contact on as-grown GaAsSb (272-HBT structure) for different pad spacings.	35
3.14	I-V curve for metal (Ti/Pt/Au) contact on as-grown GaAsSb (400-HBT structure) for different pad spacings.	36
3.15	Plot showing the dependence of resistance on the spacing between the pads. TLM test patterns were formed on both as-grown and Zn doped GaAsSb layer.	36
3.16	I-V curve for metal (Ti/Pt/Au) contact on Zn doped GaAsSb (400-HBT structure) for different pad spacings.	38
4.1	Diffusion profiles normalized to the surface concentration and diffusion lengths. (A) $D = \text{constant}$; (B) $D \propto C$; (C) $D \propto C^2$; (D) $D \propto C^3$	41
4.2	Experimental and theoretical variation of Zn concentration with distance at 1000 °C in GaAs. The arrows indicate the “effective zero” for each theoretical curve [22].	44
4.3	SIMS and ISR data for 500 °C and 550 °C, 4 hour diffusion, and interstitial-substitutional curve fits [27].	47
4.4	Zn diffusion profiles in GaSb	49
4.5	Modeled and experimental Zn distribution profiles in test structure 233 for a 600 °C, 30 minute diffusion.	53
4.6	Modeled and experimental Zn distribution profiles in test structure 233 for a 600 °C, 15 minute diffusion.	53
4.7	Modeled and experimental Zn distribution profiles in test structure 233 for a 600 °C, 5 minute diffusion.	54

TABLES

2.1	EFFECT OF SPIN SPEED ON ZINCSILICAFILM THICKNESS AFTER CURING.	9
2.2	ERROR ANALYSIS OF HALL-EFFECT MEASUREMENTS.	12
2.3	INSTRUMENT CONDITIONS FOR SIMS.	14
2.4	HBT LAYER STRUCTURE GROWN BY MOCVD, WAFER ID 272 (272-HBT).	14
2.5	HBT LAYER STRUCTURE GROWN BY MBE, WAFER ID 400 (400-HBT).	15
2.6	ETCH SEQUENCE FOR MAKING TLM TEST PATTERN ON 272-HBT STRUCTURE.	16
3.1	VARIATION OF DIFFUSION DEPTH AND ZINC ACTIVATION WITH DIFFUSION CONDITIONS	28
3.2	TLM MEASUREMENT RESULTS ON GaAaSb BASE LAYER. . .	37

ACKNOWLEDGMENTS

I express my deep sense of gratitude and sincere thanks to my advisor Dr. Patrick Fay, who gave me the opportunity to work in the fascinating area of III-Vs and Diffusion. He has been a constant source of motivation throughout the course of my research at Notre Dame. I am grateful to him for always being supportive of the experiments I wanted to carry out and also for his guidance and suggestions on my work.

Thanks to Rajkumar for helping me deal with device processing issues, to Sun for helping me with characterization in B-26 and his help with Unix, to Xiang Li for his suggestions and help with mask fabrication, to Wu Bin for her help with SEM, to Yogesh for his help with Latex among other things and Bo Yang for the fun and laughter.

I am thankful to Dr. Seabaugh and Dr. Jena for their consent to be on my committee. I would like to thank Dr. Kosel for the discussion on my work when I was getting nowhere.

Thanks to all my friends and my roommates - Praveen, Anupam and Harish who made my stay at Notre Dame an enjoyable and memorable one.

CHAPTER 1

INTRODUCTION AND MOTIVATION

High-speed device technologies are needed for many advanced systems. For example, integrated circuits for transmission at 40 Gb/s have been developed and are currently under test for long haul optical communications [1]. Emergence of 160 Gb/s transmission equipment in the near future would require significant improvement in bandwidth of the semiconductor electronics. Another example includes mixed signal ICs such as analog to digital converters, digital to analog converters and direct digital synthesizers, which are constantly being pushed to obtain wider bandwidths and higher resolution. High resolution ADCs and DACs require transistor bandwidths 10^2 to 10^4 times larger than the signal frequencies involved. Consequently, these mixed signal ICs require transistors with current gain cut-off frequency, f_T , and maximum frequency of oscillation, f_{MAX} , to be several hundred GHz [2].

InP based HBTs are among the front-runners when it comes to achieving large bandwidth because they combine the superior material properties of InP and the intrinsic speed advantage of bipolar transistors. HBTs grown on InP substrates offer high electron velocity, which leads to shorter transit times, a low turn-on voltage thereby minimizing power consumption, a large valence band discontinuity at the base-emitter junction to suppress hole injection and increase current gain, and are compatible with 1.3–1.55 μm lightwave communication systems [3]. Bipolar transistors offer potential speed advantages over other device technologies because the

carrier transport depends on the vertical dimension which is easier to scale as compared to the field-effect transistors where the carrier transport is lateral and depends on the lithographic scaling. Bipolar transistors also have high transconductance and enable faster switching for digital applications.

InP/InGaAs based HBTs have been widely investigated and have demonstrated excellent frequency performance - current gain cut-off frequency in excess of 400 GHz has been demonstrated [4]. However, $\text{In}_{0.53}\text{Ga}_{0.47}\text{As}$ is a narrow band gap material ($\Delta E_g = 0.75$ eV) [5], and its use as the collector material results in a low breakdown voltage. Wide band gap materials such as $\text{Al}_{0.48}\text{In}_{0.52}\text{As}$ or InP can be used as the collector and they enhance the breakdown voltage because of reduced impact ionization. However, the junction between the narrow band gap $\text{In}_{0.53}\text{Ga}_{0.47}\text{As}$ base and the wider band gap InP collector exhibits a positive conduction band discontinuity, which degrades device performance. At the emitter base junction this spike results in higher turn-on voltage and at the collector base junction this offset causes current blocking. The blocking effect increases carrier storage in the base and reduces f_T , and also enhances base recombination thereby decreasing the current gain. This effect can be reduced by compositional grading, incorporation of setback layers, and/or doping at the base-collector junction, but this complicates transistor design and imposes stringent uniformity and repeatability requirements on epitaxial growth [5].

The InP/GaAsSb material system presents an attractive alternative to the InP/InGaAs junction for implementation of DHBTs due to its staggered band line up. At 300 K, the $\text{GaAs}_{0.51}\text{Sb}_{0.49}$ conduction band edge lies 0.15 eV above that of InP and enables the implementation of abrupt B/C collector heterojunctions, which do not suffer from the collector current blocking effect that plagues InGaAs based DHBTs [5]. Figure 1.1 shows the energy band diagram of the $\text{GaAs}_{0.51}\text{Sb}_{0.49}$ base

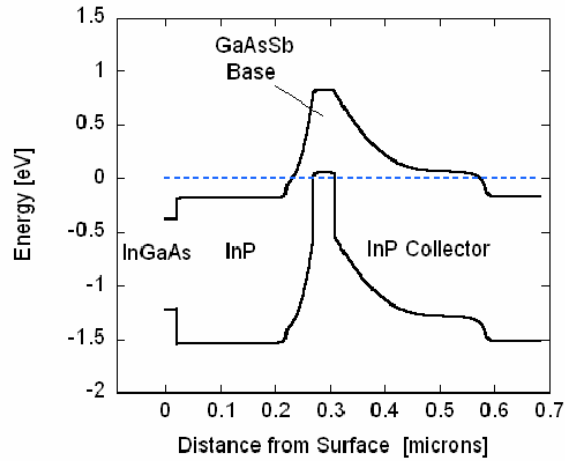


Figure 1.1. Equilibrium band diagram for InP/GaAs_{0.51}Sb_{0.49}/InP DHBT.

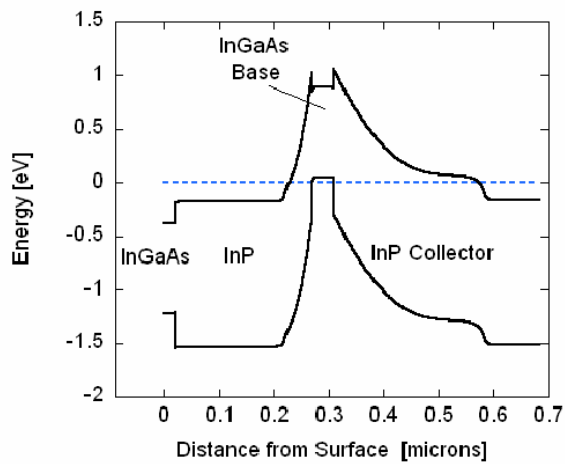


Figure 1.2. Equilibrium band diagram for InP/In_{0.53}Ga_{0.47}As/InP DHBT.

DHBT and Figure 1.2 shows the band diagram for a similar structure if the base layer was replaced by In_{0.53}Ga_{0.47}As and no compositional grading was employed. The advantages of the InP/GaAsSb heterojunction are clearly seen: the abrupt B/C junction does not have any current blocking effect and enables higher collector in-

jection velocity and shorter transit times. In addition, this structure leads to a large discontinuity in the valence band at the B/E junction ($\Delta E_v = 0.78$ eV) [5], which works to our advantage and leads to reduced hole back injection which increases the emitter efficiency. Bolognesi *et al.* [6] have demonstrated InP/GaAs_{0.51}Sb_{0.49}/InP DHBTs exhibiting peak f_T of 305 GHz and f_{MAX} of 300 GHz on a $0.4 \times 11 \mu\text{m}^2$ emitter device with a 200 Å base. The base doping level was $8 \times 10^{19} \text{ cm}^{-3}$ and typical base sheet resistance value determined by TLM measurements was 1400 Ω/sq. They also reported a small area $0.25 \times 11 \mu\text{m}^2$ emitter device with a breakdown voltage $BV_{CEO} \geq 6$ V and a common-emitter current gain $\beta = 30\text{--}40$ with a 250 Å base and 2000 Å InP collector layer. These results demonstrate that abrupt junction InP/GaAs_{0.51}Sb_{0.49}/InP DHBTs exhibit excellent frequency performance as well as high breakdown voltage.

One of the major drawbacks of InP/GaAsSb/InP DHBTs is the high value of base sheet resistance due to the low hole mobility $\mu_P = 20\text{--}30 \text{ cm}^2/\text{Vs}$ in GaAs_{0.51}Sb_{0.49}. McDermott *et al.* [7] have reported that hole mobility in GaAsSb is roughly 50–60 % of that in InGaAs for a given doping concentration. If one assumes that a similar trend holds for minority-carrier electrons, then in order to achieve the same f_T the base width in GaAsSb-base HBTs would have to be around half the base width of InGaAs-base HBTs. This scaling in base width further increases the base resistance for GaAsSb HBTs. High base sheet resistance represents a major challenge for GaAsSb based DHBTs because it necessitates the use of smaller geometry devices to achieve higher f_{MAX} . Base sheet resistance can be decreased by increasing the doping level (typically carbon) in the GaAsSb base during growth but this will lead to reduction in current gain due to Auger recombination [8], [9]. A technique that will minimize the sheet resistance of the base without effecting the current gain of the transistor is hence needed to make further improvements in f_{MAX} . Post growth

selective doping of the extrinsic base region of the transistor is one such approach to reduce the base sheet resistance without effecting the transport in the intrinsic region of the device.

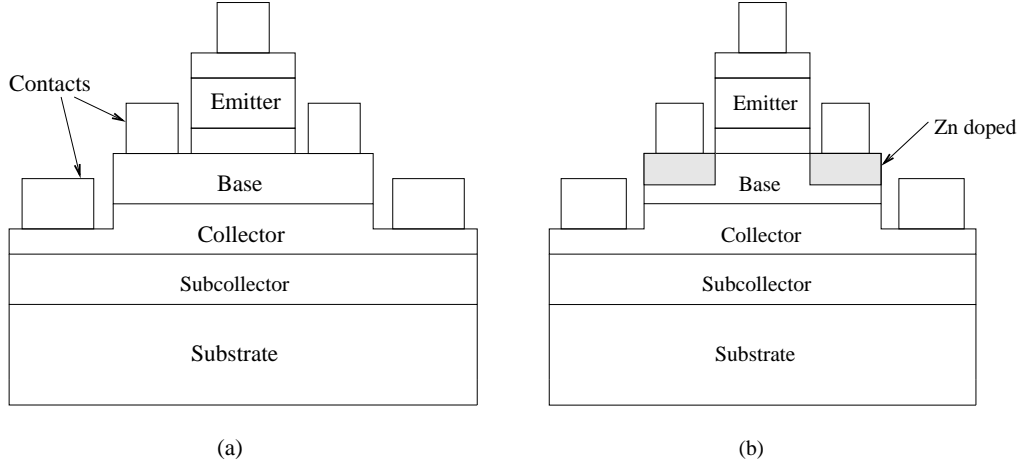


Figure 1.3. (a) Cross section of a conventional HBT fabricated by mesa etch process. (b) Cross section of HBT showing additional dopants in the extrinsic base introduced by a spin-on dopant process.

In the present work, Zn diffusion in GaAsSb from spin-on glass dopant sources is evaluated to accomplish post-growth doping of the extrinsic base region of GaAsSb-base HBTs. Diffusion from spin-on glass sources is attractive because it can be carried out without the need for sealed ampoule processing. The spin-on glass layer, which is essentially a SiO_2 film containing the dopant atoms, serves to cap the semiconductor surface and prevent the outdiffusion of volatile group V elements and supplies dopant atoms at the same time. Spin-on glass films are also easy to pattern and allow diffusion in selected areas. Figure 1.3(a) shows the cross section of the conventional HBT fabricated by a three mesa etch process. Figure 1.3(b) shows the cross section of the HBT fabricated by incorporating the spin-on dopant technique in the process to selectively dope the extrinsic base region of the transistor. The Zn

doped region will have a higher carrier density and will thus have a reduced sheet resistance. Higher concentration under the base metal will also improve the contact resistance with the base metal. Hence, we predict improvement in the maximum current gain cut-off frequency (f_{MAX}) of the transistor.

This work establishes the process conditions for diffusion of Zn in GaAsSb. Studies are undertaken to see the effect of Zn incorporation on the electronic transport properties of GaAsSb. Zn distribution profiles in undoped GaAsSb are modeled to get insight into the mechanism of Zn diffusion in GaAsSb and to predict the Zn profiles for other diffusion conditions.

CHAPTER 2

EXPERIMENTAL PROCEDURE

Experiments that were performed can be broadly classified in the following two categories:

1. **Diffusion Experiments:** To establish the process conditions for diffusion of Zn in GaAsSb and to investigate the diffusion mechanism.
2. **TLM Experiments:** To establish Zn concentration and activation in the GaAsSb-base layer of the InP/GaAsSb/InP DHBT structure for improving the electronic transport properties of GaAsSb base layer for high speed applications.

2.1 Diffusion Experiments

Zn diffusion in GaAsSb was investigated by means of Hall-effect measurements and SIMS analysis. The test structure for these experiments consisted of a 2000 Å thick GaAsSb layer grown on a semi-insulating InP substrate by MOCVD and lattice matched to InP. The epitaxial growth temperature of GaAsSb was 538–540 °C. GaAsSb was pre-doped with carbon which acts as a p-type impurity. Two test structures, with wafer identity numbers 233 and 236, with different background hole concentrations were used.

233: Hole Concentration = $2.05 \times 10^{16} \text{ cm}^{-3}$, and

236: Hole Concentration = $9.65 \times 10^{17} \text{ cm}^{-3}$

The hole concentration was measured using the van der Pauw technique at room temperature.

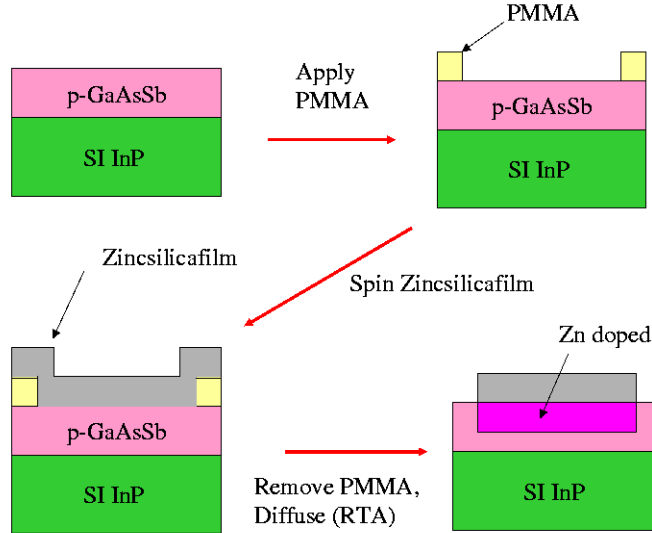


Figure 2.1. Processing steps for Zn diffusion from spin-on glass films.

Although the GaAsSb base layer used in typical HBT structures is doped to very high levels ($> 10^{19} \text{ cm}^{-3}$), lower doped test structures were chosen to facilitate Hall-effect measurements and to clearly show the effect of post growth Zn incorporation from the spin-on diffusants.

2.1.1 Sample Preparation

Wafers were cleaved into samples of square geometry. Sample sizes were approximately $4 \times 4 \text{ mm}^2$ for the 233 structure, and $6 \times 6 \text{ mm}^2$ for the 236 structure. Samples underwent processing as illustrated in Figure 2.1 and described in detail below.

(a) *Solvent Clean*: Samples were cleaned in warm acetone and iso-propyl alcohol (IPA) for 5 minutes each and blown dry with N_2 .

(b) *Protect Sample Corners*: To define the area for making indium contacts on the sample corners for Hall measurements to be carried out later, PMMA was applied to the sample corners followed by baking at $200 \text{ }^\circ\text{C}$ for 2 minutes to evaporate the

solvents.

(c) *Spin Zincofilm*: Samples were dipped in dilute HCl (HCl:H₂O::1:2) for 10 seconds to etch any oxides that may have formed on the surface of the wafer after exposure to air. This was followed by a dehydration bake at 200 °C for 2 minutes. This procedure improves the adhesion of Zincofilm [10] to the sample surface and prevents it from cracking after it is cured. Immediately after the bake, Zincofilm is spun on to the wafer at speeds ranging from 2000–5000 rpm for a time of 30 seconds. Following this, the sample was cured at 200 °C for 15 minutes to drive away the solvents and leave a film of glass doped with zinc atoms. Table 2.1 shows the thickness of the Zincofilm spun at different speeds and measured by step profiling. For the diffusions performed in this study, Zincofilm was spun at 4000 rpm. High acceleration of 10,000 rpm/s was used in all the samples because it resulted in good quality films which did not crack.

Table 2.1

EFFECT OF SPIN SPEED ON ZINCOFILM THICKNESS AFTER CURING.

Spin speed (rpm)	Time (s)	Average Film Thickness (Å)	Result
2000	30	3207	Film cracks
3000	30	3371	Film cracks
4000	30	2892	Does not crack
5000	30	2612	Does not crack

(d) *Diffusion in a Rapid Thermal Processor*: Once the film is spun on the sample and it is cured, the sample is ready for the diffusion process. Diffusions were carried in a rapid thermal processor (RTP) to exercise strict control over the diffusion time

and temperature, and to let transient enhanced diffusion (TED) work in our favor. TED occurs when the temperature of the sample is changed abruptly and leads to diffusion enhancement [11]. The samples were kept on top of a silicon wafer which was placed on quartz pins and heated by high intensity halogen lamps. A thermocouple in contact with the silicon wafer was used to measure the temperature. The sample was kept directly above the thermocouple in order to accurately read the temperature for the duration of the diffusion. The thermal ramp rate was kept constant at 50 °C/s for diffusion temperatures up to 650 °C, and no cracking of the spin-on glass film was observed after rapid thermal processing. Figure 2.2 shows a typical temperature profile during a diffusion.

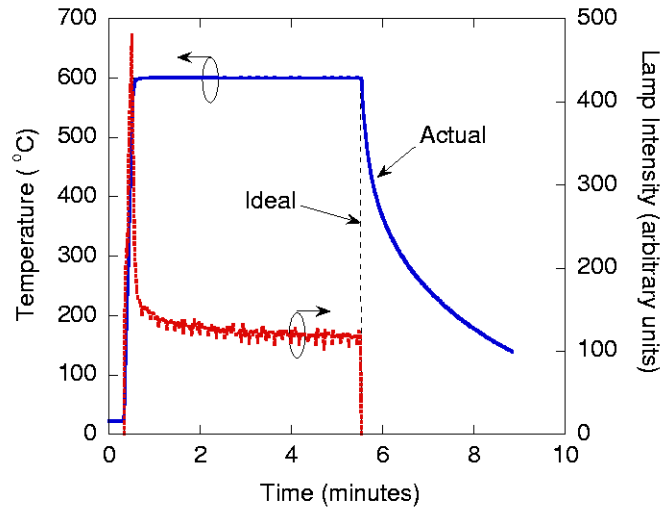


Figure 2.2. Typical temperature profile during rapid thermal diffusion.

2.1.2 Hall-effect Measurements

Hall-effect measurements were carried out using the Van der Pauw technique both before (on some samples) and after rapid thermal annealing. Indium was used to make contacts to the four corners of the square sample. Care was taken to ensure

that indium was applied only to a small area on the corners and it did not touch the sides of the wafer. Four gold wires of 99.9% purity and diameter 5 mil were used to draw out the contacts and were bonded to the sample using indium. Samples were attached to a holder by winding the gold wire around the four screws and vacuum grease was applied between the sample and the holder plate to act as a mild adhesive to hold the sample in the same plane as the holder plate. Resistance between each of the four contacts was measured and Hall-effect measurements were performed only if the resistance between any two contacts was within a factor of two of the others. The holder was then placed in between two poles of the electromagnet such that the magnetic field was normal to the sample. A computer program controlled the magnitude and direction of the magnetic field and was interfaced with current source, nano-voltmeter, and a switching box. Current, as specified by the user, flowed between two terminals from the current source and voltage between the other two was read from the nano-voltmeter. An algorithm, based on the van der Pauw technique [12], [13] was used by the computer program, which calculated and returned the values of mobility, resistivity, sheet resistance and carrier concentration.

Most of the measurements were performed at room temperature. Low temperature measurements were performed for some of the samples by immersing the holder plate in liquid nitrogen.

2.1.3 Error Analysis for Hall-effect Measurements

To determine the error in the measurements, 10 measurements were performed on sample (236 structure) of size 6×6 mm² under the same conditions. The results of the measurements are presented in Table 2.2, which shows that the error in measurement due to the noise in the system is negligible and the measurements are repeatable.

Table 2.2

ERROR ANALYSIS OF HALL-EFFECT MEASUREMENTS.

	Mean	Standard Deviation	Error
Carrier Concentration	$1.071 \times 10^{18} \text{ cm}^{-3}$	$2.618 \times 10^{15} \text{ cm}^{-3}$	0.25 %
Sheet Resistance	4829.9 ohm/sq.	5.23 ohm/sq.	0.11 %
Hole mobility	$60.35 \text{ cm}^2/\text{Vs}$	$0.18 \text{ cm}^2/\text{Vs}$	0.30 %

From sample to sample, the error in the measurement can arise due to:

1. Error in the measurement of magnetic field. This is estimated to be 2 % and translates to 2 % error in determination of carrier concentration and mobility.
2. Finite size of the indium contacts at the edge of the sample as shown in Figure 2.3. If the average diameter of the contact is 'd' and the length of the sample is 'L', the error in the measurement is of the order of 'd/L' [13]. The average diameter of the contact is estimated to be 0.8 mm. Hence, error in the measurement of 233 samples ($L = 4 \text{ mm}$) is approximately $0.8/4 \times 100 = 20\%$, and in 236 samples ($L = 6 \text{ mm}$) error is approximately $0.8/6 \times 100 = 13.3\%$

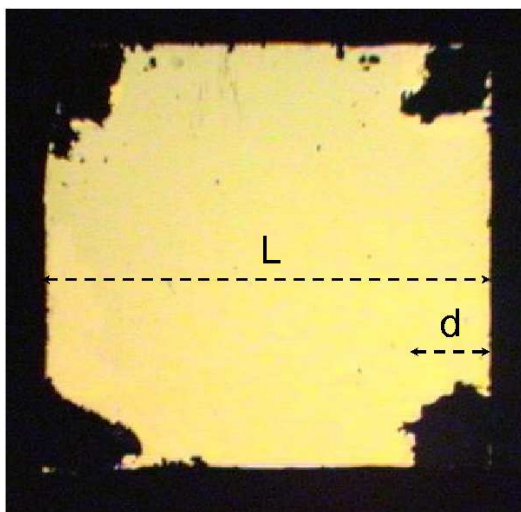


Figure 2.3. Sample used for Hall-effect measurements showing the average diameter 'd' of the indium contacts and the dimension 'L' of its edge. The error in measurement due to finite size of the contact is of the order of 'd/L' [13].

These two sources of error are independent of each other and the total percentage error is given by the square root of the sum of squares of each error. This value is used to make the error bars in the plots of hole concentration, sheet resistance and mobility.

2.1.4 SIMS Analysis

After performing Hall-effect measurements, samples were cleaned in methylene chloride, acetone, and isopropyl alcohol (IPA) in that order to remove the vacuum grease. Zincsilicafilm was removed by treating the samples with buffered HF for 1–2 minutes followed by a rinse in DI water. The surface was examined under an optical microscope for any evidence of surface degradation. SIMS analysis was performed on these samples by Charles Evans and Associates [14].

A low primary ion beam energy of 1 keV was used for SIMS analysis. The samples were analyzed for Zn with Ga, As, Sb and P as matrix markers. The detection limit of Zn for this analysis was 10^{17} atoms/cm³. The quantification of Zn was done by concurrent analysis of a GaAs standard. Quantification was based on relative sensitivity factors (RSF) determined from the analysis of known standards. The depth scale was quantified by measuring the analysis craters with a stylus profilometer. The instrumental conditions for the experiment are summarized in the Table 2.2.

Table 2.3

INSTRUMENT CONDITIONS FOR SIMS.

<i>Elements Monitored</i>	P, Zn, Ga, As, Sb
<i>Primary Ion Beam</i>	Cs
<i>Primary Ion Energy</i>	1 keV
<i>Secondary Ion Polarity</i>	Positive

[†]Used for accurate analysis of insulating samples or substrates.

2.2 TLM Experiments

TLM experiments were performed to investigate the effect of incorporating Zn in the GaAsSb base layer on the base contact resistance and the sheet resistance. The HBT test structures, wafer identifier 272 grown by MOCVD (epitaxial growth temperature was 538–540 °C) and wafer identifier 400 grown by MBE, were used for these experiments and their corresponding layer structures are shown in Tables 2.4 and 2.5.

Table 2.4

HBT LAYER STRUCTURE GROWN BY MOCVD, WAFER ID 272 (272-HBT).

Layer	Material	x	Thickness(Å)	N_D (cm ⁻³)	Dopant
7	n-In _{x} Ga _{1-x} As	0.47	200	1.20×10^{19}	Te
6	n-InP		2000	8.00×10^{18}	Si
5	n-InP		500	5.00×10^{17}	Si
4	p-GaAs _{x} Sb _{1-x}	0.49	400	3.00×10^{19}	C
3	n-InP		2750	4.00×10^{16}	Si
2	n-InP		5450	7.00×10^{18}	Si
1	i-InP		100	-	Si

Table 2.5

HBT LAYER STRUCTURE GROWN BY MBE, WAFER ID 400 (400-HBT).

Layer	Material	Thickness(Å)	N_D (cm^{-3})
7	n-InGaAs	1000	3×10^{19}
6	n-InP	1000	3.00×10^{19}
5	n-InP	700	3.00×10^{17}
4	p-GaAsSb	400	4.00×10^{19}
3	n-InP	3000	3.00×10^{16}
2	n-InGaAs	500	3.00×10^{19}
1	n-InP	3000	3.00×10^{19}

2.2.1 Sample Preparation

Wafers were cleaved into samples of size $5 \times 5 \text{ mm}^2$ and subjected to the following processing:

(a) *Solvent Clean*: Samples were cleaned in warm acetone and IPA for 5 minutes each and blown dry with N_2 .

(b) *Blanket Emitter Etch*: The entire emitter, layers 5,6, and 7, is removed by etching, without any mask, to expose the base layer. The etch sequence used is shown in Table 2.6. In this etch sequence, dilute HCl is used to remove the oxide that forms on the surface of the sample upon exposure to air. After the InP etch using H_3PO_4 :HCl solution, the sample is treated with concentrated HCl for 5–10 seconds to ensure that InP is removed completely and also to dissolve the quaternary material layers at the InP/GaAsSb interface. HCl does not etch GaAsSb and the base layer remains intact.

(c) *Define TLM Mesa*:

- Dehydration bake at $120 \text{ }^\circ\text{C}$ for 5 minutes
- Spin photoresist (PR) AZ5214E at 5000 rpm for 30 seconds
- Pre-bake at $110 \text{ }^\circ\text{C}$ for 30 seconds

Table 2.6

ETCH SEQUENCE FOR MAKING TLM TEST PATTERN ON 272-HBT
STRUCTURE.

Layer	Thickness	Etchant	Etch Rate	Time
Oxide	-	HCl(1):H ₂ O(2)	-	15 s
InGaAs	200/1000 Å	H ₃ PO ₄ (15):H ₂ O ₂ (5):H ₂ O(200)	30-60 Å/s	20/60 s
InP	2500/1700 Å	H ₃ PO ₄ (9):HCl(1)	60-110 Å/s	60/60 s
InP	-	HCl(2):H ₂ O(1)	~ 8μm/min	5-10 s

- Edge bead removal
- Expose to ultraviolet (UV) light in Karl Suss MJB contact aligner using TLM Mesa mask with dose of 125 mJ/cm²
- Develop in AZ327 for 30 seconds, observe under microscope and develop as necessary
- Post bake at 120 °C for 1 minute

(d) *Mesa Etch:* Etch 400 Å of GaAsSb in H₃PO₄(15):H₂O₂(5):H₂O(200) for 1 minute. Etch InP in H₃PO₄(9):HCl(1) solution for 10 seconds to etch a few hundred Angstroms of InP to provide better isolation of the mesas as the InP layer is doped to a low level of 4×10^{16} cm⁻³. Remove the photoresist and measure mesa height.

(e) *Define TLM Pads:*

- Dehydration bake at 120 °C for 5 minutes
- Spin PR AZ5214E at 5000 rpm for 30 seconds
- Pre-bake at 110 °C for 30 seconds
- Edge bead removal
- Expose to UV light in Karl Suss aligner using TLM Pad mask with dose of 75 mJ/cm²
- Reversal bake at 110 °C for 60 seconds
- Flood expose without mask at 220 mJ/cm²
- Develop in AZ327 for 30 seconds, observe under microscope and develop as necessary.

(f) *Metal Deposition and Lift Off:* 200 Å of Ti, 500 Å of Pt and 2000 Å of Au is evaporated on the sample surface. Acetone is sprayed on the sample to remove

the photoresist and metal not in contact with the semiconductor surface. Sample is then rinsed in IPA and blown dry.

2.2.2 TLM Measurements

After the test samples were prepared, the spacing between the TLM contact pads was measured by optical microscopy. The contact resistance measurement setup consisted of a DC probe station with four tungsten probes of $1.2\ \mu\text{m}$ diameter for making contacts to the sample. An HP3457A multimeter was used for the 4-probe measurement of resistance between the metal pads and a Solaris workstation was used to control the multimeter through the GPIB interface and for extraction of parameters from the measured data. A current of 1 mA was used to determine the voltage between the metal pads. The measured spacing between the pads for each sample was used in the data analysis.

CHAPTER 3

RESULTS AND DISCUSSION

The results of the diffusion experiments and TLM experiments are presented and discussed in this chapter.

3.1 Results of Diffusion Experiments

Diffusion of Zn in GaAsSb was characterized by Hall-effect measurements and SIMS analysis. Data obtained by these techniques is presented below.

3.1.1 Hall-effect measurements

Figure 3.1 shows the hole concentration plotted with respect to the diffusion time for temperatures ranging from 500–600 °C for the structures 233 and 236 with different background doping. Figures 3.2 & 3.3 show a similar plot for the corresponding sheet resistance and mobility. As seen from Figure 3.1, at a temperature of 500 °C, as the diffusion time increases from zero (i.e. before any diffusion) to 5, 15 and 30 minutes no significant change in hole concentration is observed. As the diffusion temperature increases to 550 °C, the hole concentration in 236 is seen to increase from $9.65 \times 10^{17} \text{ cm}^{-3}$ to $2.17 \times 10^{18} \text{ cm}^{-3}$ for diffusion carried out for half an hour. Correspondingly, sheet resistance decreases from $4.59 \times 10^3 \text{ } \Omega/\text{sq.}$ to $3.41 \times 10^3 \text{ } \Omega/\text{sq.}$ due to increase in the number of carriers while the hole mobility is reduced to $40 \text{ cm}^2/\text{Vs}$ from an initial value of $67 \text{ cm}^2/\text{Vs}$. These results, when combined with

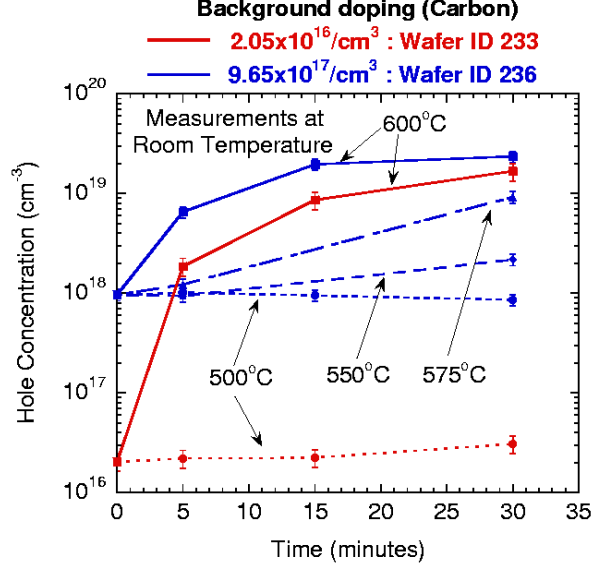


Figure 3.1. Hole concentration with respect to Zn diffusion time for temperatures ranging from 500–600 °C for the structures 233 and 236 with different background doping.

the results of SIMS profiling to be discussed in the next section, imply that the threshold temperature at which Zn atoms becomes electrically active in GaAsSb is in the range of 500–550 °C. As the diffusion temperature is further increased to 600 °C, the hole concentration increases by almost three orders of magnitude for the 233 structure with lower background doping. Sheet resistance for this sample decreases from 265 k Ω /sq. to 906 Ω /sq. and the mobility reduces to 22 cm²/Vs from 59 cm²/Vs.

The minimum sheet resistance observed is 358 Ω /sq. for 600 °C, 30 minutes diffusion. It is to be noted, however, that this value is for a 2000 Å thick GaAsSb layer which is considerably thicker than the base widths commonly employed in HBTs. A typical value for base width used in DHBT layer structures is 400 Å. If diffusions were carried out in a 400 Å thick layer with the same background doping level of

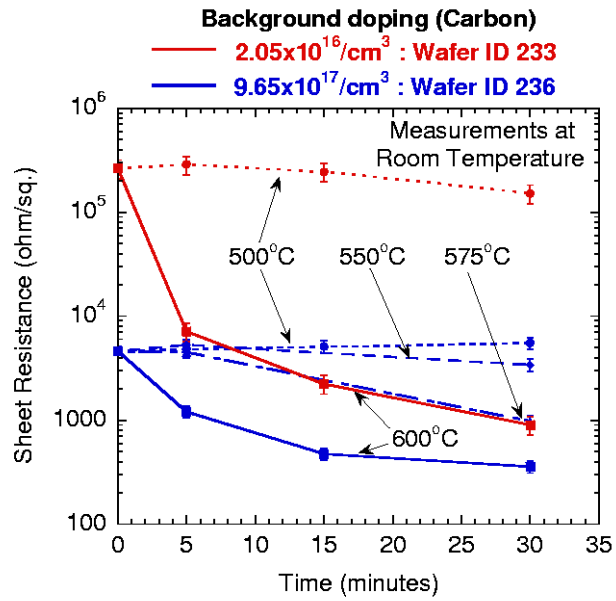


Figure 3.2. Sheet resistance with respect to Zn diffusion time for temperatures ranging from 500–600 °C for the structures 233 and 236 with different background doping.

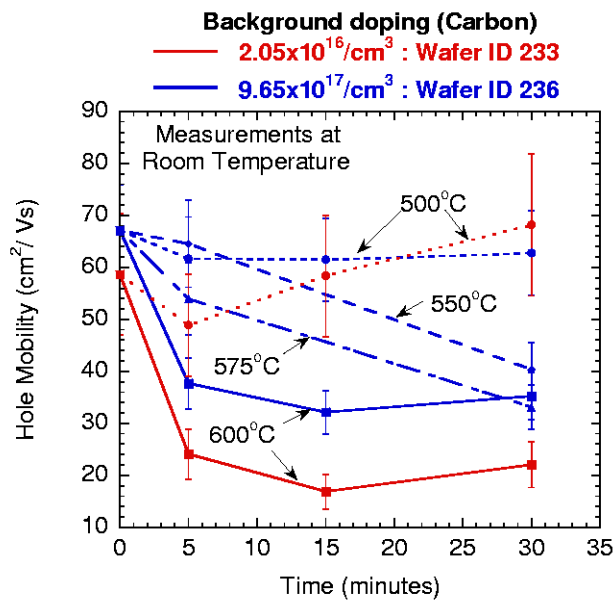


Figure 3.3. Mobility with respect to Zn diffusion time for temperatures ranging from 500–600 °C for the structures 233 and 236 with different background doping.

$9.65 \times 10^{17} \text{ cm}^{-3}$ we would expect the sheet resistance to be $1790 \text{ } \Omega/\text{sq}$. An actual typical value of sheet resistance for a $400 \text{ } \text{\AA}$ thick InGaAs base layer (carbon doping: $6 \times 10^{19} \text{ cm}^{-3}$) is $560 \text{ } \Omega/\text{sq}$. [17], whereas, for the 272-HBT structure (Table 2.4) GaAsSb base ($400 \text{ } \text{\AA}$ thick and carbon doped to $3 \times 10^{19} \text{ cm}^{-3}$) the measured sheet resistance is $2044 \text{ } \Omega/\text{sq}$. From Figure 3.2 it is seen that sheet resistance decreases as the background doping in GaAsSb increases. With the background doping of $3 \times 10^{19} \text{ cm}^{-3}$ in the GaAsSb base layer of the 272-HBT structure, the sheet resistance after Zn diffusion is expected to decrease further below $1790 \text{ } \Omega/\text{sq}$. and approach the value of sheet resistance for InGaAs bases with similar doping and thickness.

From Figure 3.1, it is also seen that the hole concentration in structure 236 is higher than that in structure 233 for the same diffusion conditions, implying that Zn diffuses faster as the background doping increases. Here it is assumed that diffusion takes place from an infinite source. Further evidence of this will be presented in section 3.1.2, where SIMS profiles are presented.

Figure 3.3 shows that mobility decreases as the hole concentration increases due to the diffusion of Zn in the GaAsSb layer. Low temperature Hall-effect measurements at 77 K performed on the sample in which Zinc diffusion was carried out at $600 \text{ } ^\circ\text{C}$ for 15 minutes, resulted in a mobility of $29.7 \text{ cm}^2/\text{Vs}$, whereas the room temperature mobility was $24.9 \text{ cm}^2/\text{Vs}$. The low-temperature mobility is thus only 20% higher than the room temperature mobility. This modest temperature dependence suggests that the decrease in mobility due to increase in hole concentration may be due to relatively temperature insensitive ionized impurity scattering. It is also observed from the figure that the mobility dependence on hole concentration is modest for concentrations in excess of $1 \times 10^{18} \text{ cm}^{-3}$. For structure 236, $\mu_p = 37.5 \text{ cm}^2/\text{Vs}$ for $N_A = 6.5 \times 10^{18} \text{ cm}^{-3}$ and $\mu_p = 35.5 \text{ cm}^2/\text{Vs}$ for $N_A = 2.4 \times 10^{19} \text{ cm}^{-3}$.

3.1.2 SIMS Profiles

Figure 3.4 shows the evolution of Zn profiles as the diffusion temperature increases from 500 to 600 °C. At 500 °C, Zn is incorporated in the sample only in the thin surface layer. At a temperature of 550 °C, the Zn profile extends up to a depth of 1000 Å for a 30 minute diffusion. Diffusion of Zn is also consistent with the observed increase in hole concentration from $9.65 \times 10^{17} \text{ cm}^{-3}$ to $2.17 \times 10^{18} \text{ cm}^{-3}$ for a 550 °C, 30 minute diffusion as seen in Figure 3.1. For diffusions performed at 600 °C, Zn profiles in structure 236 extend deeper compared to those in structure 233. At 600 °C, Zinc thus diffuses faster in the sample with higher background doping. This is also consistent with the Hall-effect measurements where higher carrier concentration is obtained for 236 samples for the same set of diffusion conditions. An explanation of why this takes place will be presented in Chapter 4, where the mechanism of Zn diffusion in GaAsSb is discussed.

Figures 3.5 and 3.6 show the evolution of Zn profiles with both time and temperature for the structures 233 and 236, respectively. As expected, the diffusion front extends deeper into the sample as the diffusion time increases. In Figure 3.5 consider the Zn diffusion profiles at 550 °C and 575 °C. The profiles for 30 minute diffusion exhibit a plateau region which is a characteristic of isothermal steady-state diffusion. The profiles for shorter diffusion times of 5 minutes are steep and do not show a distinct plateau region which is indicative of the diffusion taking place under non-equilibrium conditions. The occurrence of the plateau region agrees with the findings of Kamanin *et al.* [15]. Figure 3.7 shows the experimental Zn diffusion profiles in n-type InP for diffusion carried out at 450 °C under the initial diffusion stage (heating time of 3 minutes), curve 1, and for an isothermal diffusion for 30 minutes, curve 2, which shows a distinct plateau region. Even though the mecha-

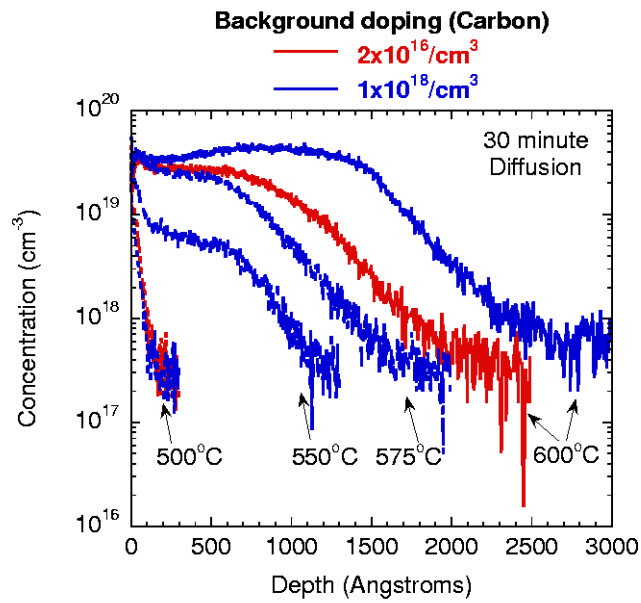


Figure 3.4. Zn profile for a 30 minute diffusion at temperatures ranging from 500–600 °C.

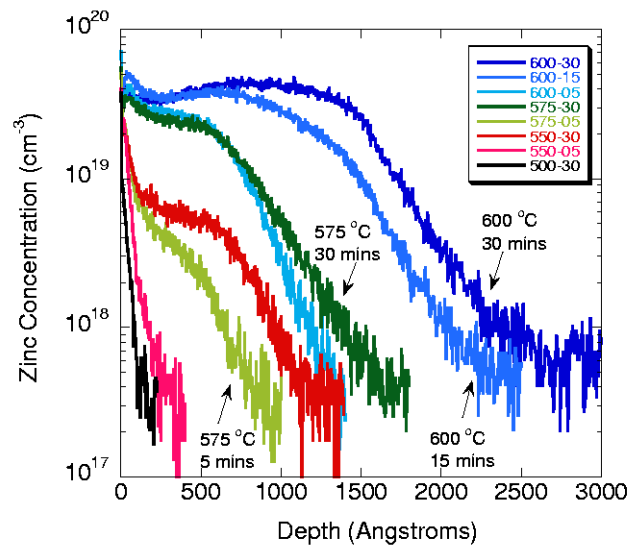


Figure 3.5. Zn distribution profiles in structure 236 for temperatures ranging from 500–600 °C.

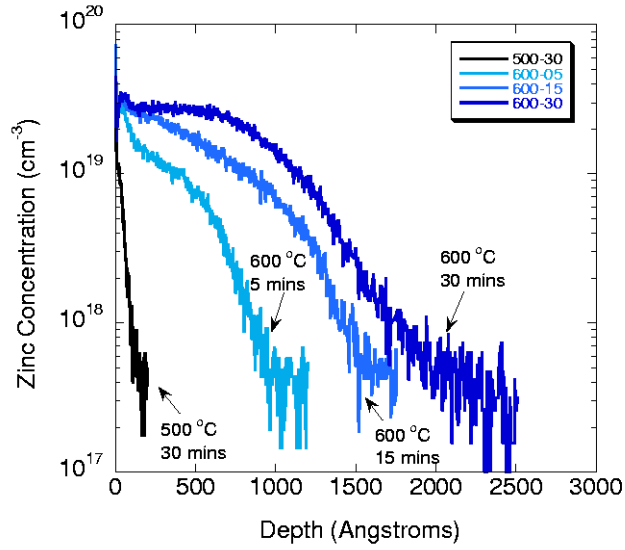


Figure 3.6. Zn distribution profiles in structure 233 for temperatures 500 °C and 600 °C.

nism by which Zn diffuses in InP may be completely different from that in GaAsSb, Figure 3.7 shows how Zn profile after isothermal diffusion is expected to be different from the one obtained after diffusions for short durations. From Figure 3.5 it is also observed that as the diffusion temperature increases, the concentration at which the plateau forms approaches the surface Zn concentration. In structure 233, for a 600 °C, 30 minute diffusion concentration of the plateau region is same as the surface Zn concentration. This implies that surface concentration of Zn atoms can be increased by increasing the diffusion temperature until the surface concentration reaches the concentration of the source or the solid solubility limit of Zn in GaAsSb at that temperature. The time taken for the sample inside the RTP to reach thermal equilibrium can be roughly estimated from the temperature profile shown in Figure 2.2 for a 600 °C, 5 minute diffusion. The thermocouple takes 0.64 seconds to reach a constant temperature of 600 °C. Since the thermocouple is placed just

beneath the sample and there is no change in the system once the thermocouple reaches a constant temperature, it can be assumed that the the sample reaches thermal equilibrium within 0.64 seconds. This time is very small compared to the diffusion times of 5 to 30 minutes used in the diffusion experiments and we can consider the sample to be at thermal equilibrium throughout the diffusion process. It takes significantly longer for the vacancies and interstitials to reach equilibrium concentration inside the sample as seen from the SIMS profiles. Vacancy equilibrium is further discussed in section 4.4 where the Zn diffusion profiles in GaAsSb are modeled.

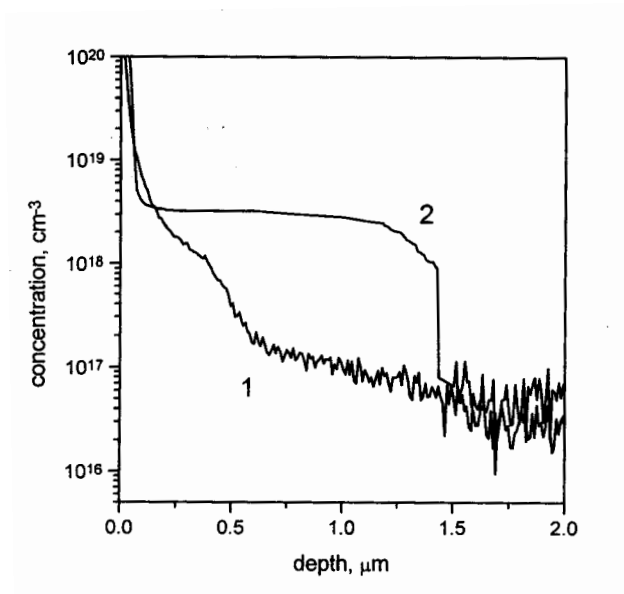


Figure 3.7. Plot showing the initial diffusion stage (IDS) and steady state Zn distribution (450 °C, 30 minute diffusion) profile in InP (Kamanin *et al.* [15]).

Zn diffusion profiles in GaAsSb exhibit a gradual diffusion front in contrast to a step diffusion front observed for Zn diffusion in GaAs and in GaSb (compare Figures 3.4, 4.2 and 4.4). In the SIMS profiles shown in Figure 3.4, the slope of the diffusion front does not appear to change as Zn diffuses beyond the GaAsSb layer

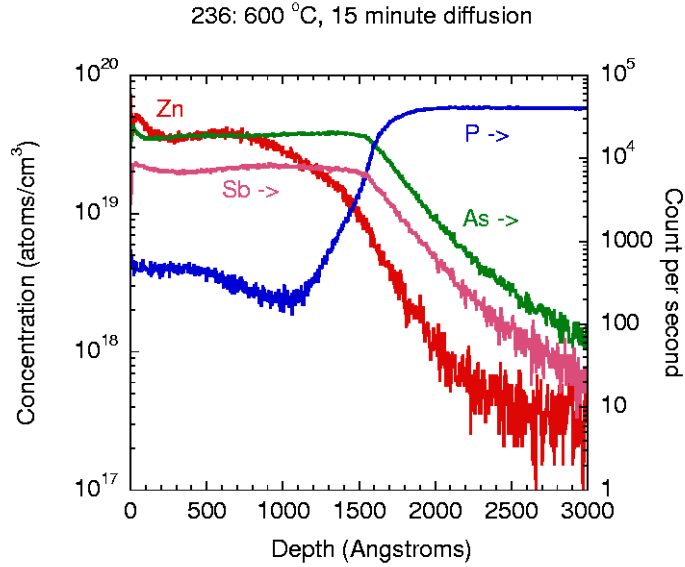


Figure 3.8. Plot showing Zn, In, As, Sb profiles in 2000 Å GaAsSb on InP. Zn diffusion was carried out at 600 °C for 30 minutes.

into the InP substrate. As shown in Figure 3.4, a 500 °C, 30 minute Zn diffusion into GaAsSb results in less than 200 Å diffusion depth, while Kamanin *et al.* [15] have reported that for a 450 °C, 30 minute diffusion, Zn profile extends up to 1500 Å in InP (refer Figure 3.7). Consequently, Zn profiles are expected to be steeper in GaAsSb than in InP because Zn diffuses considerably faster in InP as compared to GaAsSb. The absence of a kink in the Zn diffusion profile at the GaAsSb/InP interface may be due to the interface not being abrupt. This is especially true when the diffusions are performed at high temperatures that cause mixing of the interface. Figure 3.8 shows the SIMS distribution profile of Zn, As, Sb and P in structure 236 after performing rapid thermal diffusion at 600 °C for 15 minutes. Profiles of As, Sb and P are not abrupt during the transition from GaAsSb material to InP, instead they change gradually and there is significant mixing at the interface. For structure 236, the thickness of the GaAsSb layer as determined by step profiling after etching

GaAsSb in $\text{H}_3\text{PO}_4(15):\text{H}_2\text{O}_2(5):\text{H}_2\text{O}(200)$ is 2100 Å. This suggests that transition from GaAsSb to InP occurs over a distance of several hundred angstroms, from approximately 1500 Å to 2100 Å.

3.1.3 Zinc Activation

Zn activation can be calculated from the Hall-effect measurements and SIMS profiles. Hall-effect measurements give the hole concentration in the sample before and after Zn is diffused. The increase in the hole concentration after diffusion is due to the Zn atoms that get substitutionally incorporated into the GaAsSb lattice and become electrically active. SIMS, on the other hand, quantifies the Zn atoms in the sample and allows us to calculate the total Zn dose. This allows us to calculate Zn activation, as described below. Zn activation, diffusion depth and Zn concentration per unit area both before and after rapid thermal diffusion are tabulated in Table 3.1.

Table 3.1

VARIATION OF DIFFUSION DEPTH, HOLE CONCENTRATION BEFORE & AFTER ZINC DIFFUSION AND ZINC ACTIVATION WITH DIFFUSION TIME AND TEMPERATURE FOR TEST STRUCTURES 233 AND 236.

Temp. (°C)	Time (minutes)	Depth (Å)	[Hole] _{BeforeRTP} (cm ⁻²)	[Hole] _{AfterRTP} (cm ⁻²)
Test Structure 236				
500	30	119	2.02×10^{13}	1.80×10^{13}
550	5	240	2.02×10^{13}	1.87×10^{13}
550	30	1140	2.02×10^{13}	4.54×10^{13}
575	5	850	2.02×10^{13}	2.56×10^{13}
575	30	1680	2.02×10^{13}	1.93×10^{14}
600	5	1450	2.02×10^{13}	1.37×10^{14}
600	15	2500	2.02×10^{13}	4.11×10^{14}
600	30	2800	2.02×10^{13}	4.95×10^{14}
Test Structure 233				
500	30	160	4.00×10^{11}	6.04×10^{11}
600	5	960	4.00×10^{11}	3.65×10^{13}
600	15	1860	4.00×10^{11}	1.68×10^{14}
600	30	2370	4.00×10^{11}	2.90×10^{14}

Temp. (°C)	Time (minutes)	Δ [Hole] (cm ⁻²)	[Zn] _{Total} (cm ⁻²)	Zn Activation (%)
Test Structure 236				
500	30	-2.20×10^{12}	4.35×10^{12}	-50.6
550	5	-1.50×10^{12}	1.39×10^{13}	-10.8
550	30	2.52×10^{13}	5.70×10^{13}	44.2
575	5	5.40×10^{12}	3.62×10^{13}	14.9
575	30	1.73×10^{14}	2.12×10^{14}	81.5
600	5	1.17×10^{14}	2.15×10^{14}	54.3
600	15	3.91×10^{14}	4.86×10^{14}	80.4
600	30	4.75×10^{14}	6.37×10^{14}	74.5
Test Structure 233				
500	30	2.04×10^{11}	6.34×10^{12}	3.2
600	5	3.61×10^{13}	8.59×10^{13}	42.0
600	15	1.68×10^{14}	1.92×10^{14}	87.5
600	30	2.90×10^{14}	2.91×10^{14}	99.6

In Table 3.1,

- Depth is the depth from the surface at which Zn concentration falls to $1 \times 10^{17} \text{ cm}^{-3}$ (the sensitivity level of the SIMS profile measurement),
- $[\text{Zn}]_{\text{Total}}$ denotes the total concentration of Zn atoms in the sample,

$$[\text{Zn}]_{\text{Total}} = \int_{x=0}^{\text{Depth}} [\text{Zn}(x)] dx$$

Here, the upper limit of integration is the depth from the surface at which Zn concentration falls to $1 \times 10^{17} \text{ cm}^{-3}$. The integration is limited at this value by the sensitivity limit of the SIMS profiler.

- $[\text{Hole}]_{\text{BeforeRTP}}$ denotes the hole concentration as measured by Hall-effect in the sample before diffusion,
- $[\text{Hole}]_{\text{AfterRTP}}$ denotes the hole concentration as measured by Hall-effect in the sample after diffusion,
- $\Delta[\text{Hole}]$ denotes the change in hole concentration after diffusion,

$$\Delta[\text{Hole}] = [\text{Hole}]_{\text{AfterRTP}} - [\text{Hole}]_{\text{BeforeRTP}}$$

- Zn activation is the percentage of the total Zn atoms that are electrically active in the sample with the assumption that the background hole concentration due to Carbon does not change after the diffusions are carried out.

$$\text{Activation} = \frac{\Delta[\text{Hole}]}{[\text{Zn}]_{\text{Total}}} \times 100\%$$

It has been reported by McDermott *et al.* [16] that when carbon-doped GaAsSb layers lattice matched to InP were subjected to annealing at 400 to 450 °C in a nitrogen ambient, no measurable hydrogen passivation was detected. Post-anneal measurements performed by them typically showed hole concentrations at approximately the same level as the as-grown lattice matched samples. In calculating Zn activation, it is assumed that the hole concentration of the carbon-doped lattice-matched GaAsSb layer (structures 233 and 236) do not change up to a temperature of 600 °C for times up to 30 minutes.

Figure 3.9 shows the plot of Zn activation with respect to the diffusion conditions. Activation takes both positive and negative values. A negative activation implies that hole concentration after diffusion is less than that of as-grown sample. Similarly, for positive activation the hole concentration is higher than that in the as-grown sample. For diffusions performed below 550 °C, Zn atoms are largely

inactive. This affirms the conclusion drawn from the Hall-effect measurement results that the threshold temperature at which Zinc atoms become electrically active in GaAsSb is in the range of 500–550 °C. Below this temperature Zn atoms may largely exist as interstitials or as charged or neutral complexes. Higher activation is observed for diffusion in the lower doped structure 233 and activation increases as the diffusion time and temperature are increased, as one would expect. Increasing the temperature of diffusion increases the Ga vacancy and interstitial concentration as well as the diffusivity of Zn atoms. This makes it more favorable for a Zn atom to occupy a Ga site. Increasing the diffusion time permits a larger number of Zn atoms to be incorporated.

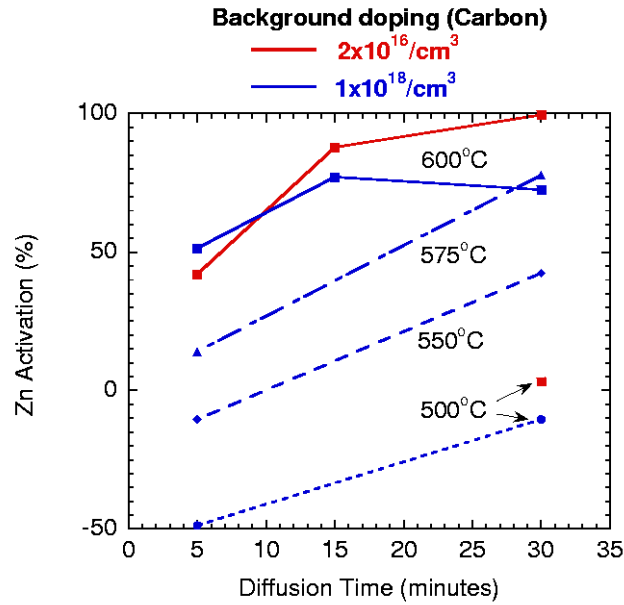


Figure 3.9. Zn activation in structures 233 and 236 with respect to the diffusion conditions.

Negative activation may be due to compensation by interstitial Zn atoms since Zn_i^+ is a donor. Negative activation is also possible if the Zn atoms form a complex with the surrounding atoms and/or defects in the lattice resulting in the complex

having a net positive charge.

3.2 Zinc Diffusion in 400 Å GaAsSb Base Layer for HBT Application

Diffusion experiments (section 2.1) were carried out with the aim of establishing process conditions for diffusion of Zn in GaAsSb. Test structures 233 and 236 were chosen to facilitate this study as they had a thicker GaAsSb layer that was doped lightly as compared to the base layer in a typical HBT, which is heavily doped. Before the spin-on dopant process can be employed in HBT processing to improve the transport properties of a GaAsSb base, optimum diffusion conditions have to be established for the thinner and heavily doped GaAsSb base layer of the 272-HBT structure. It is also desired that the:

- Zn profile is confined to the thin base layer so that Zn does not cross over to the InP collector,
- Zn activation should be high to increase the hole concentration, and
- Thermal budget should be small to prevent the mixing of the epitaxial layers at the interface.

With this aim, rapid thermal diffusions were performed at high temperatures in order to achieve high activation and for short durations to confine Zn to the thin base layer and keep the thermal budget low. Diffusions performed at 600 °C for 30 s, 60 s and at 625 °C for 30 s yielded SIMS distribution profiles as shown in Figures 3.10, 3.11 and 3.12, respectively. These diffusion conditions significantly reduce the mixing at the heterojunction interface, as the Ga, As, Sb and P profiles are fairly abrupt in all cases. Zn profiles are also box shaped and do not extend beyond the GaAsSb layer. Zn dose increases from $5.08 \times 10^{13} \text{ cm}^{-2}$ (for diffusion at 600 °C, 30 seconds) to $6.49 \times 10^{13} \text{ cm}^{-2}$ (for diffusion at 600 °C, 60 seconds). For diffusion at still higher temperature of 625 °C for 30 s, Zn dose was considerably more at $1.09 \times 10^{14} \text{ cm}^{-2}$. These results, however, do not reveal what percentage of these Zn

atoms are electrically active. The heavily-doped GaAsSb base layer and the presence of conducting layers below the base makes interpretation of the Hall-effect measurement data a difficult task. The Hall-effect measurements performed on a sample having several conducting layers give the effective values of carrier concentration, sheet resistance and mobility because conduction takes place through all the layers. For example, Hall-effect measurements performed on as-grown GaAsSb layer after removing all the emitter layers of the 272-HBT structure result in n-type material with carrier concentration of $7.91 \times 10^{19} \text{ cm}^{-3}$, sheet resistance of $16.04 \text{ } \Omega/\text{sq.}$ and mobility of $1230 \text{ cm}^2/\text{Vs}$. A thickness of 400 \AA was used for calculations and the current was kept at 0.5 mA . After Zn diffusion is performed at $625 \text{ }^\circ\text{C}$ for 30 s , the corresponding values of carrier concentration, sheet resistance and mobility are $7.79 \times 10^{19} \text{ cm}^{-3}$, $16.14 \text{ } \Omega/\text{sq.}$, and $1240 \text{ cm}^2/\text{Vs}$. The latter values fall well within 2% of the former values and this difference may arise because of the 10% measurement error from sample to sample. Hence, it is difficult to single out the effect of Zn diffusion on GaAsSb base layer. Instead, TLM measurements are performed on these samples which give the base sheet resistance and contact resistance. TLM measurements are discussed in section 3.3.

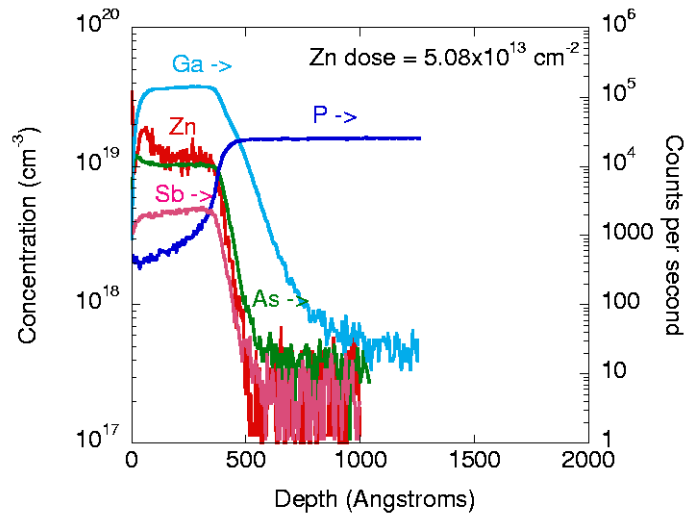


Figure 3.10. SIMS distribution profile of Zn, Ga, As, Sb and P in 272-HBT GaAsSb base layer after a 600 °C, 30 s rapid thermal diffusion.

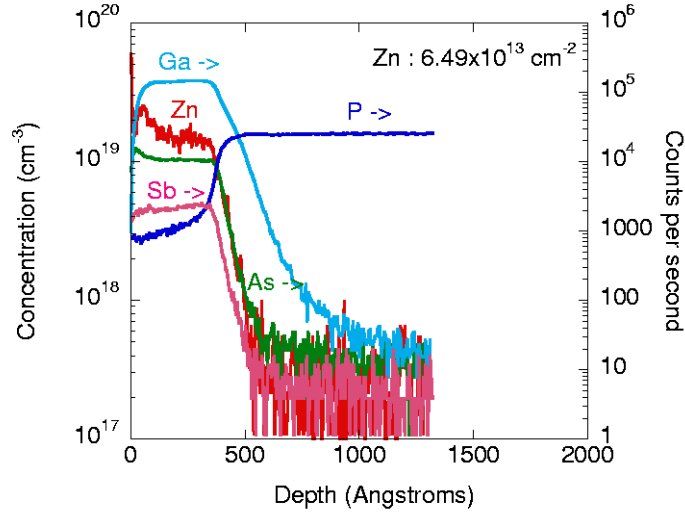


Figure 3.11. SIMS distribution profile of Zn, Ga, As, Sb and P in 272-HBT GaAsSb base layer after a 600 °C, 60 s rapid thermal diffusion.

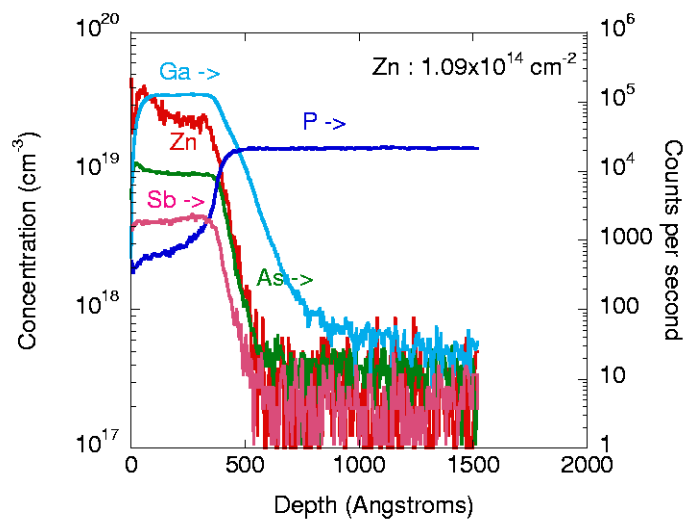


Figure 3.12. SIMS distribution profile of Zn, Ga, As, Sb and P in 272-HBT GaAsSb base layer after a 625 °C, 30 s rapid thermal diffusion.

3.3 Results of TLM Measurements

In this section, the results of TLM experiments are presented. Two structures, 272-HBT (grown by MOCVD) and 400-HBT (grown by MBE), were used for these experiments. Zn diffusions from spin-on glass films were carried out in the GaAsSb base layer at temperatures of 600 and 625 °C for durations 30, 45 and 60 seconds. TLM test patterns were made on both as-grown and Zn doped GaAsSb layer.

Figures 3.13 and 3.14 show that the I-V curves for the metal contacts formed on as-grown GaAsSb are linear for both 272-HBT and 400-HBT structures. This implies that the contacts are ohmic. The resistance between the metal pads is also seen to increase linearly with the gap length in Figure 3.15. The results of measurements are presented in Table 3.3.

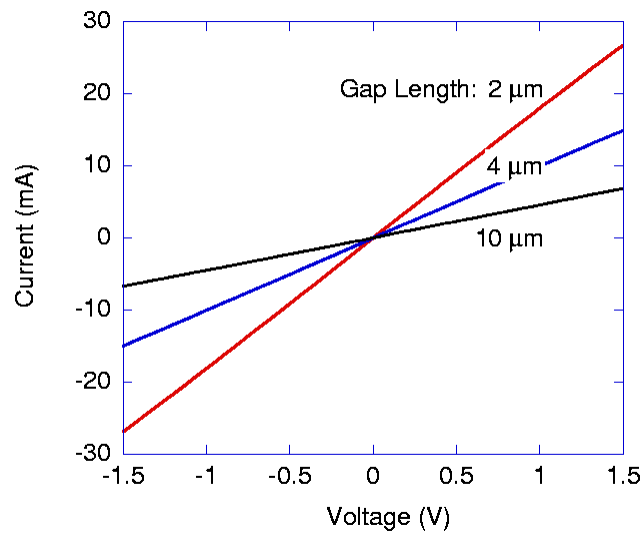


Figure 3.13. I-V curve for metal (Ti/Pt/Au) contact on as-grown GaAsSb (272-HBT structure) for different pad spacings.

For the TLM test pattern made on 272-HBT structure, measurements reveal that the rapid thermal diffusions performed at 600 °C cause an increase in the value

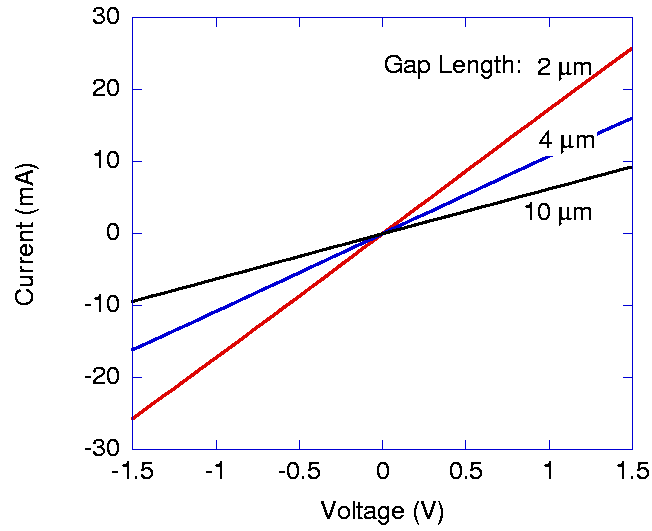


Figure 3.14. I-V curve for metal (Ti/Pt/Au) contact on as-grown GaAsSb (400-HBT structure) for different pad spacings.

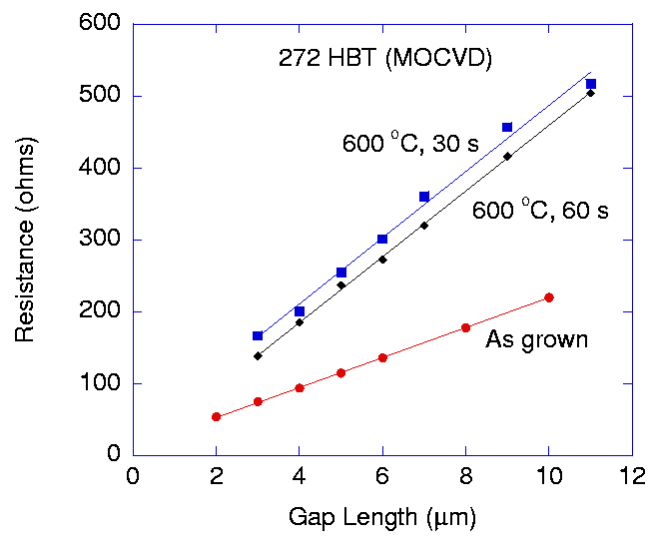


Figure 3.15. Plot showing the dependence of resistance on the spacing between the pads. TLM test patterns were formed on both as-grown and Zn doped GaAsSb layer.

Table 3.2

TLM MEASUREMENT RESULTS ON GaAsSb BASE LAYER.

Diffusion conditions	Sheet Resistance ($\Omega/\text{sq.}$)	Contact Resistance (Ωmm)	Specific Contact Resistance (Ω/cm^2)	Lin. Corr. Coefficient
272-HBT structure				
As-grown	2044.4	0.633	1.962×10^{-6}	0.9996
600 °C, 30 s	4602.3	1.337	3.884×10^{-6}	0.9962
600 °C, 60 s	4569.4	1.075	2.529×10^{-6}	0.9996
625 °C, 30 s	n/d	n/d	n/d	n/d
400-HBT structure				
As-grown	1221.6	1.183	1.145×10^5	0.9994
625 °C, 30 s	n/d	n/d	n/d	n/d
625 °C, 60 s	n/d	n/d	n/d	n/d

n/d: could not be determined from TLM measurements.

of sheet resistance as compared to that of the as-grown GaAsSb layer. This may be because the Zn dopant atoms are not electrically activated and they form complexes with the surrounding defects or atoms thereby reducing the hole concentration. In order to increase the activation of Zn atoms, diffusion temperature was increased to 625 °C and the diffusion time was kept as 45 seconds. However, it was observed that resistance between the gaps varied from 1.29 to 1.71 k Ω and the resistance did not increase linearly with the spacing between the pads. This value is much higher than the resistance observed in the as-grown GaAsSb layer (Figure 3.15). A similar trend was observed when diffusions were performed at 625 °C for the 400-HBT structure. The resistance between the pads was found to be several kilohms and showed lot of scatter. I-V characteristics of the contact between the metal and Zn doped GaAsSb were found to be non-linear as shown in Figure 3.16.

During the fabrication of TLM test patterns it was also observed that the

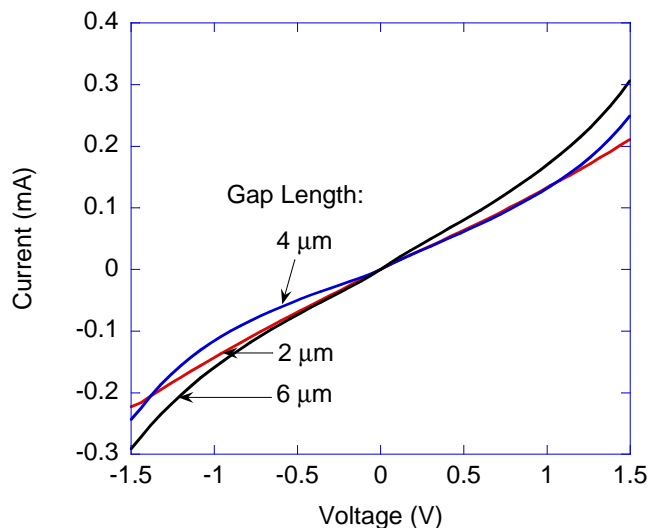


Figure 3.16. I-V curve for metal (Ti/Pt/Au) contact on Zn doped GaAsSb (400-HBT structure) for different pad spacings.

GaAsSb layer which was doped with Zn did not etch easily in $\text{H}_3\text{PO}_4(15):\text{H}_2\text{O}_2(5):\text{H}_2\text{O}(200)$, which etches as-grown GaAsSb selectively. This may be due to the high concentration of Zn atoms in the GaAsSb layer and/or due to the mixing of the heterojunction interface due to treatment at higher temperatures.

Although attractive in theory, the idea of reducing the sheet resistance of a heavily doped thin GaAsSb layer by diffusing Zn atoms using spin-on dopant technique could not be demonstrated in practice. The exact cause of this is unknown but it may be due to the complex formation which reduces the hole concentration or mixing of the heterojunction interface, as discussed above.

CHAPTER 4

DIFFUSION MODELING

In this chapter, a brief introduction to simple diffusion theory is given. A review of some of the important work on Zinc diffusion in related III-V semiconductors (GaAs and GaSb) is presented, knowledge of which is of help in understanding the Zn diffusion in GaAsSb. A model which describes Zn diffusion in undoped GaAsSb is proposed to explain the experimental results. Zinc diffusivity values at the surface and in the bulk GaAsSb are obtained by fitting the experimental data.

4.1 Diffusion in III-V Semiconductors [19]

Diffusion theory as described by Tuck [19] is discussed in this section. Diffusion occurs in the presence of a concentration gradient of mobile atoms. In general, the atoms will move in such a way as to remove the gradient. The simplest assumption which can be made is that the flux of atoms at any point is in the direction opposite of the concentration gradient and proportional to the flux, i.e.

$$J = -D\nabla C. \quad (4.1)$$

where J is the flux of atoms at the point (x, y, z) , C is the concentration at the same point and D is the constant of proportionality, usually called the diffusion coefficient. Equation (4.1) is usually called Fick's law. In one dimension the law

becomes

$$J_x = -D \frac{\partial C}{\partial x}. \quad (4.2)$$

D is a function of temperature and is given by the relation

$$D = D_0 \exp -\frac{E_A}{kT} \quad (4.3)$$

where E_A is the activation energy required for an atom to jump from one stable position in a crystal to the next. The continuity condition requires that

$$\frac{\partial C}{\partial t} = \frac{\partial}{\partial x} D \frac{\partial C}{\partial x}. \quad (4.4)$$

for the one-dimensional case. If D is a constant, then equation (4.4) becomes

$$\frac{\partial C}{\partial t} = D \frac{\partial^2 C}{\partial x^2} \quad (4.5)$$

The solution to equation (4.5) depends on the boundary conditions, i.e. on the experimental conditions employed during the diffusion process. If, for instance, a sample initially contains no dopant and the experimental procedure imposes a surface concentration C_0 throughout the diffusion, the boundary conditions become

$$\left. \begin{array}{ll} C = 0 & x > 0, t = 0 \\ C = C_0 & x = 0, t > 0 \end{array} \right\} \quad (4.6)$$

for which the solution takes the form of a complementary error function:

$$C = C_0 \operatorname{erfc} \frac{x}{2\sqrt{Dt}}. \quad (4.7)$$

A normalized erfc profile is shown in Figure 4.1 curve A. In practice, the diffusion profiles found in experiments often do not coincide with any of the well-known solutions to equation (4.5) [19]. Mathematically this can be dealt with by assuming a variable D so that solutions are sought to equation (4.4) rather than equation (4.5). In Figure 4.1, curves B, C and D correspond to $D \propto C$, $D \propto C^2$, and $D \propto C^3$,

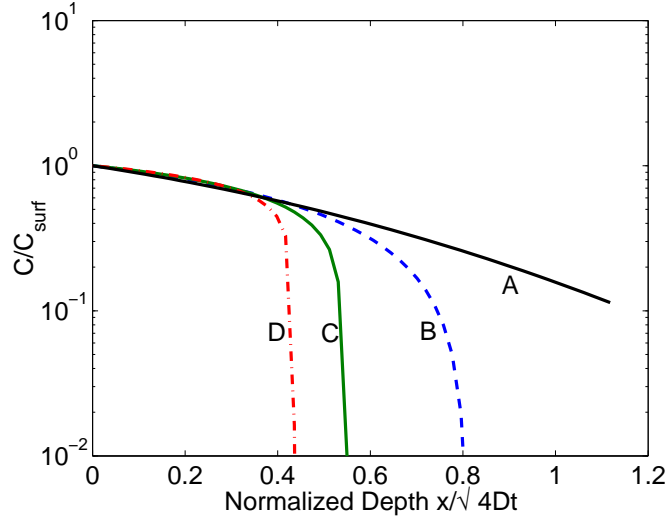


Figure 4.1. Diffusion profiles normalized to the surface concentration and diffusion lengths. (A) $D = \text{constant}$; (B) $D \propto C$; (C) $D \propto C^2$; (D) $D \propto C^3$.

respectively. With increasing dependence on C the impurity distribution profiles become steeper upto an almost abrupt transition from the doped layer towards the substrate. However, physical reasons must be sought to explain the non-constant value of D . Usually, it proves to be due to the complexity of the diffusion mechanism involved. Impurities can exist in a semiconductor in more than one form: charged or uncharged, for instance, or as individual atoms and as constituents of complexes. Usually these different forms will diffuse differently and, in addition, there will be interactions between them. This leads to D varying in a complicated way even at constant temperature and the concept of diffusion coefficient becomes rather less useful.

4.2 Diffusion of Zn in GaAs [19]

This section presents the work on Zn diffusion in GaAs as described by Tuck [19]. Early work done in the 1960's in which diffusion profiles were measured for Zn in III-

V's indicated that the diffusion profiles did not correspond to solutions of equation (4.5). The rate of diffusion appeared to depend on concentration and a profile often showed a concave section. The diffusion front was invariably sharp.

It was proposed by Longini [21], that a substitutional-interstitial mechanism could be used to account for the Zn/GaAs results. This model assumes that Zn can exist in two different forms in the GaAs crystal: as an interstitial, in which case it acts as a donor, Zn_i^+ , and also as substitutional acceptor on the Ga site, Zn_{Ga}^- . The model also assumes that most of the impurity is in the substitutional form but this species has a negligible diffusion coefficient [21]. Diffusion therefore proceeds by movement of the highly mobile interstitial atom. This process is concentration-dependent because the proportion of Zn which is in the interstitial state increases with total concentration. This is because the concentration of substitutional Zn, Zn_{Ga}^- , depends on the concentration of Ga vacancies which remain constant in a crystal under thermal equilibrium. A simple relationship exists describing the transition between the two forms:



where h^+ is a hole. According to this equation, a Zn interstitial combines with a Ga vacancy and occupies it producing two free holes. If we can make the assumption that this reaction comes to equilibrium at a rate which is fast compared to the diffusion rate, the law of mass action can be applied:

$$K_2 p^2 [\text{Zn}_{\text{Ga}}^-] = [\text{Zn}_i^+] [\text{V}_{\text{Ga}}] \quad (4.9)$$

which is true throughout the crystal. Here K_2 is a constant and p denotes the hole concentration. By postulating that $[\text{Zn}_{\text{Ga}}^-] \gg [\text{Zn}_i^+]$, then in order for the crystal to remain neutral, $p \simeq [\text{Zn}_{\text{Ga}}^-]$ and equation (4.9) becomes

$$K_2 [\text{Zn}_{\text{Ga}}^-]^3 = [\text{Zn}_i^+] [\text{V}_{\text{Ga}}]. \quad (4.10)$$

If we call the concentrations of substitutional Zn, interstitial Zn and Ga vacancies C_s , C_i and C_v respectively then equation (4.10) becomes

$$K_2 C_s^3 = C_i C'_v \quad (4.11)$$

where the prime indicates that the concentration of Ga vacancies is constant at the equilibrium value throughout the crystal [19]. This assumption will be examined later. C_s and C_i are functions of x and t , with equilibrium values C'_s and C'_i at the surface, which are maintained by the various phases outside the sample. Thus at $x = 0$

$$K_2 C'^3_s = C'_i C'_v. \quad (4.12)$$

Since the substitutional species is assumed to be essentially immobile [21], any increase in either substitutional or interstitial Zn inside the semiconductor is due to diffusion of interstitial atoms, i.e.

$$\frac{\partial C_i}{\partial t} + \frac{\partial C_s}{\partial t} = D_i \frac{\partial^2 C}{\partial x^2} \quad (4.13)$$

where D_i is the diffusion coefficient of interstitials. The quantity C_i can be replaced by C_s using equation (4.11), giving

$$\left(\frac{3K_2 C_s^2}{C'_v} + 1 \right) \frac{\partial C_s}{\partial t} = D_i \frac{\partial}{\partial x} \left(\frac{3K_2 C_s^2}{C'_v} \frac{\partial C_s}{\partial t} \right). \quad (4.14)$$

If K_2 is substituted on the left-hand side using equation (4.12), it is seen that the first term in the bracket is small compared to unity. Equation (4.14) therefore simplifies to

$$\frac{\partial C_s}{\partial t} = \frac{\partial}{\partial x} \left(\frac{3K_2 D_i}{C'_v} C_s^2 \frac{\partial C_s}{\partial t} \right). \quad (4.15)$$

This is of the form of equation (4.4) with

$$D = \frac{3K_2 D_i}{C'_v} C_s^2 \quad (4.16)$$

i.e. a diffusion coefficient is obtained which is proportional to the square of the substitutional concentration. Since, by postulate, nearly all the Zn is substitutional, we effectively have $D \propto C^2$ where C is the total concentration of Zn.

Calculations based on this model were made by Weisberg and Blanc [22]. Six diffusion profiles at 1000 °C were fit using a single adjustable parameter and the results are shown in Figure 4.2.

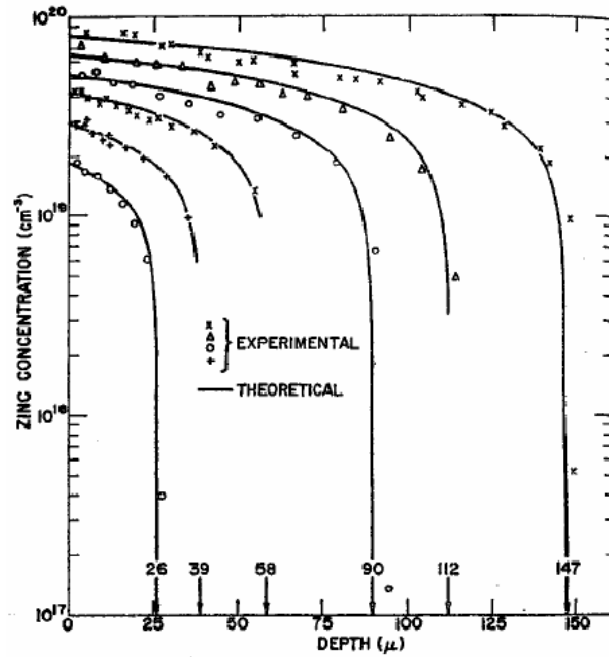


Figure 4.2. Experimental and theoretical variation of Zn concentration with distance at 1000 °C in GaAs. The arrows indicate the “effective zero” for each theoretical curve [22].

However, these calculations were done for profiles obtained using isoconcentration technique with radioisotope diffusions into uniform samples in thermal equilibrium; this theory does not give a good fit to profiles obtained by chemical diffusions. Chemical diffusions are complicated by spatially nonuniform dopant concentrations within the semiconductor, leading to built-in electric fields that can affect the dif-

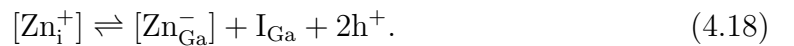
fusion profiles. The basic difference between the two types of experiment is that isoconcentration diffusions take place at thermodynamic equilibrium while chemical diffusions do not. The possibility arises, therefore, of defect equilibrium breaking down in the latter case so that equation (4.11) may not apply for chemical diffusions.

Each time equation (4.8) operates in the bulk of the semiconductor, the crystal loses a Ga vacancy. The crystal will try to maintain its equilibrium vacancy concentration by some mechanism such as dislocation climb [19], but if it is not completely successful in this, C_v will fall below C'_v inside the semiconductor. If it is assumed that the crystal has some mechanism in the bulk which produces vacancies at a rate proportional to the shortfall, in addition to equations (4.8) and (4.13) a further differential equation must be employed to describe the concentration of vacancies at a distance x from the surface:

$$\frac{\partial C_v}{\partial t} = D_v \frac{\partial^2 C_v}{\partial x^2} - \frac{\partial C_s}{\partial t} + k(C'_v - C_v) \quad (4.17)$$

where k is a constant, C_v is the concentration of Ga vacancies, C'_v is the equilibrium value of Ga vacancy concentration and D_v is the diffusion coefficient for vacancies. The first term on the right-hand side represents vacancies due to interstitial Zn going substitutional and third is the bulk production of vacancies by dislocation climb, etc. By making a number of simplifying assumptions, Tuck and Kadhim [23], were able to show that the model predicts the experimental profiles.

A different approach was suggested by Gosele and Morehead [24]. Their mechanism, which is now known as the ‘kick-out’ model has the diffusing interstitial Zn atom joining the lattice by pushing a Ga atom off its site, creating a Ga interstitial, I_{Ga} , i.e. equation (4.8) is replaced by



At thermal equilibrium the two approaches are indistinguishable, since the Ga interstitials and Ga vacancies are related by



and equation (4.17) is still obtained for diffusion coefficient. Under conditions of defect non-equilibrium, however, the models are different. In the vacancy model, the crystal has the problem of producing vacancies; in kick-out model, the problem is to eliminate excess Ga interstitials. In either case, dislocations presumably have a role to play. These two models were compared in detail by van Ommen [25], who used both approaches to fit theoretical profiles to experimental results. It was found that both models were found to give profiles of the right shape, but the kick-out model provided a better fit. It should be noted, however, that results obtained from both of these models depend critically on the assumptions made about the rate of elimination of interstitials on the one hand and production of vacancies on the other. These assumptions have been somewhat arbitrary in all the modeling carried out and the theoretical results cannot be considered as being quantitative.

4.3 Diffusion of Zn in GaSb

Kyuregyan *et al.* [26], first showed that Zn diffusion in GaSb from a constant surface concentration source cannot be described by the complementary error function. Instead, the diffusion coefficient is a function of the local zinc concentration.

Since this publication, many groups published results further exploring these initial findings, but no clear identification of the diffusion mechanism of Zn in GaSb has been made.

Conibeer *et al.* [27] proposed that Zn diffuses via a substitutional-interstitial mechanism, but they lack sufficient evidence to support either the vacancy or kick-out mechanism. They modeled the SIMS and incremental sheet resistance (ISR)

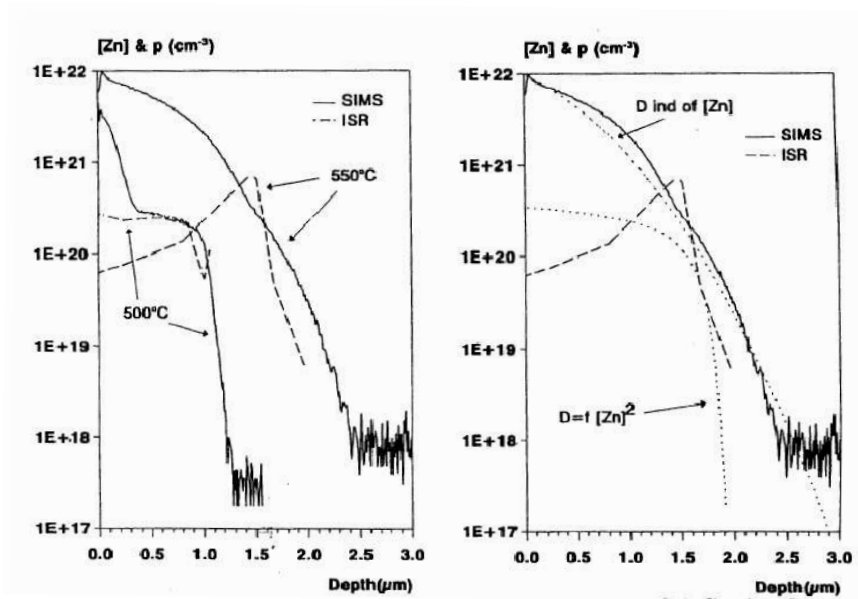


Figure 4.3. SIMS and ISR data for 500 °C and 550 °C, 4 hour diffusion, and interstitial-substitutional curve fits [27].

profile of for Zn diffusion into tellurium doped (doping level 10^{17} cm^{-3}) GaSb. Diffusions were carried out in sealed quartz glass tubes with a piece of Zn wire to act as a vapor source both with and without Sb overpressure. They used the interstitial-substitutional mechanism to model the Zn distribution profiles and assumed the reaction took place under equilibrium conditions. Hence, they did not distinguish between the two possibilities by which interstitial-substitutional mechanism can proceed, namely the vacancy and the kick-out mechanism. They also assumed that the gallium vacancy concentration, $[V_{\text{Ga}}]$ remained constant inside the crystal.

Using these assumptions they were able to obtain good fit to both SIMS and ISR profiles for 500 °C, 4 hour diffusions with the diffusivity $D_i \propto [\text{Zn}]^2$, except near the surface as shown in Figure 4.3. The SIMS curve near the surface was fit assuming D independent of $[\text{Zn}]$. At 550 °C, the ISR profiles were fit assuming $D_i \propto [\text{Zn}]^2$ and the SIMS profile were fit with D independent of $[\text{Zn}]$. They explained this behavior

by assuming that at high values of surface Zn concentration, $[Zn]_0$, a large amount of Zn diffuses in as an electrically inactive species of Zn and that it is temperature dependent, whereas the proportion moving immediately onto Zn_{Ga} sites by vacancy or kick-out reaction is largely temperature independent. They argue that these species could be mixtures of dimers or trimers, etc., and would have diffusivity between D_i and D_s . Such species will tend to diffuse in a Fickian manner until their concentration drops below that of Zn_{Ga} 's. At 500 °C, this happened fairly close to the surface; but at 550 °C, it did not occur until the knee of the Zn_{Ga} curve was reached. They calculated the diffusivity of [Zn] independent proportions of the curves as 1.1×10^{-14} at 500 °C and 1.5×10^{-13} cm²/s at 550 °C, respectively. This was the first direct comparison of total [Zn] and hole profiles in tellurium doped GaSb and it supported the interstitial-substitutional model with diffusivity dependent on $[Zn]^2$.

Nicols *et al.* [28] accurately modeled the experimental profiles for Zn concentration below 10^{20} cm⁻³ using the Ga interstitial-controlled mode of Zn diffusion via the kick-out mechanism. They performed Zn diffusion in GaSb at temperatures between 500 °C and 600 °C using Ga-Zn alloy sources. They found two kinds of profiles - kink and tail profiles for surface Zn concentrations in excess of 10^{20} cm⁻³ and box shaped profiles for surface concentrations below 10^{20} cm⁻³. They found the presence of extended defects in the samples with kink and tail profiles and did not consider them for diffusion studies. The box shaped profiles were found to be free of extended defects in the area of diffusion and could be modeled using Ga interstitial controlled mode of Zn diffusion via kick-out mechanism. In their models, they assumed that Zn diffuses interstitially as a single positively charged species, while being present as a singly ionized acceptor in the Ga substitutional position. For surface concentrations of $1 - 2 \times 10^{19}$ cm⁻³, they obtained very good fits using

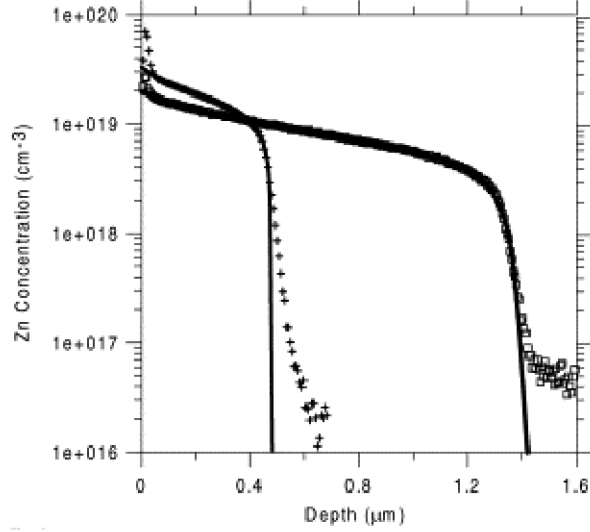
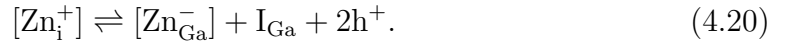


Figure 4.4. SIMS profiles and fits (solid lines) based on neutral Ga interstitial controlled mode of kick out mechanism. The samples were annealed at 609 °C for 500 min (squares) and 561 °C for 921 min (+) using a 2% Zn / 98% Ga source [28].

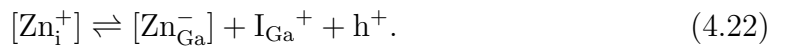
the reaction:



For surface concentrations exceeding $2 \times 10^{19} \text{ cm}^{-3}$, reaction (4.20) did not ensure an accurate fit to the Zn distribution at the diffusion front. Examples of these two distributions are shown in Figure 4.4. They pointed out that at higher surface concentration the Fermi level drops low enough to ionize the neutral Ga interstitials into a singly positively charged donor state via the reaction:



Thus, the kick-out reaction is no longer described only by reaction (4.20), but by a combination of (4.20) and the following reaction



The shallower diffusion front observed for these samples is very likely related to a lower effective rate constant for Zn_i to Zn_{Ga} exchange active at this doping level.

They extracted the diffusivity data from the fittings achieved in the surface concentration range of $1 - 2 \times 10^{19} \text{ cm}^{-3}$. Reduced Zn diffusivity data (Zn concentration independent) was used to calculate D_0 and Q for Zn diffusion under intrinsic conditions as $1.4 \times 10^{-10} \text{ cm}^2/\text{s}$ and 4.3 eV, respectively at a temperature of 609 °C. They did not rule out that singly positively charged Ga interstitials mediated Zn diffusion at doping levels of $1 - 2 \times 10^{19} \text{ cm}^{-3}$.

Although Zn diffusion in GaSb has not yet been fully established, there is enough evidence that diffusion takes place by interstitial-substitutional mechanism and of the two possibilities – vacancy and the kick-out mechanism – results favor the kick-out mechanism.

4.4 Diffusion of Zn in GaAsSb

In this section, the results of modeling the SIMS distribution profile of Zn diffusion in ‘undoped’ GaAsSb are presented. The background doping concentration in structure 233 is $2.05 \times 10^{16} \text{ cm}^{-3}$, and is much lower compared to the Zn concentration in excess of 10^{19} cm^{-3} observed near the surface in all the samples. The test structure can essentially be considered as undoped and it is likely safe to assume that the background dopant, carbon, does not play any role in diffusion of Zn. Also, the detection limit of SIMS analysis is 10^{17} cm^{-3} which is higher than the background carbon doping level in these samples.

In test structure 236, the background doping of 10^{18} cm^{-3} is comparable to the doping levels of Zn and is higher than the detection limit for SIMS analysis. Further, higher doping would change the position of the Fermi level and may change the ionization of the diffusing specie. Due to the above reasons Zn profiles in test

structure 236 have not been considered for diffusion modeling. However, these profiles are of help in verifying the diffusion model as will be seen later.

Since Zn diffuses in GaAs and GaSb by interstitial-substitutional mechanism, and GaAsSb is an alloy of GaAs and GaSb, one may assume (to start with) that Zn diffuses by the same mechanism in GaAsSb.

Let us begin with the following assumptions:

1. Zn exists in two different forms in GaAsSb: as an interstitial, in which case it acts as a donor, Zn_i^+ , and as a substitutional acceptor on the Ga site, Zn_{Ga}^- .
2. Most of the Zn is in substitutional form but this has negligible diffusion coefficient and diffusion mainly proceeds by highly mobile interstitial atom. This implies $[Zn_{Ga}^-] \gg [Zn_i^+]$, $p = [Zn_{Ga}^-] \simeq [Zn]$ and $D_i \gg D_s$, where D_i and D_s represent the diffusivity of interstitial and substitutional Zn, respectively.
3. Diffusion takes place under equilibrium conditions and vacancy equilibrium is maintained.

If diffusion proceeds by interstitial-substitutional mechanism, reaction (4.23) describes the transition between Zn interstitial and substitutional forms



The diffusion equation can be modeled along the lines of Zn diffusion in GaAs (see section 4.2) and using the above assumptions we get equations 4.24 and 4.25,

$$\frac{\partial[Zn]}{\partial t} = \frac{\partial}{\partial x} \left(D_0[Zn]^2 \frac{\partial[Zn]}{\partial t} \right) \quad (4.24)$$

$$D = D_0[Zn]^2 \quad (4.25)$$

where,

$D_0 = 3K_2D_i/[V_{Ga0}]$ is the Zn concentration independent diffusivity,

$[V_{Ga0}]$ is the Ga vacancy concentration $[V_{Ga}]$ at the surface, and

D_i is the diffusivity of Zn_i^+ .

For a 600 °C, 30 minute diffusion in test structure 233, Zn activation $\sim 100\%$ which implies that the assumption that $[\text{Zn}_{\text{Ga}}^-] \gg [\text{Zn}_i^+]$ is valid. Also, the diffusion time of 30 minutes is sufficiently long for the equilibrium to be established during the diffusion in the rapid thermal processor. In this sample, therefore, the underlying assumptions for an interstitial-substitutional mechanism are most closely met. Equation (4.24) is numerically solved for this sample for a surface Zn concentration of $3 \times 10^{19} \text{ cm}^{-3}$ (as determined from SIMS profiles) and surface diffusivity, D_{i0} , of $1 \times 10^{-13} \text{ cm}^2/\text{s}$ at 600 °C is obtained from the best fit to the experimental curve. Figure 4.5 shows that the modeled curve fits the experimental data very well up to a depth of 1000 Å. Beyond this depth, the measured Zn concentration decreases gradually instead of exhibiting a steep diffusion front that is expected from the interstitial-substitutional mechanism. Further analysis indicates that Zn diffuses in a Fickian manner beyond a depth of 1000 Å, with a concentration-independent diffusivity of $1.26 \times 10^{-14} \text{ cm}^2/\text{s}$ at 600 °C.

For a 600 °C, 15 minute diffusion, Zn activation is 87.5% (from Table 3.1) and assumptions 2 and 3 above are not so closely satisfied. This reflects in Figure 4.6 where actual Zn concentration falls slightly below the modeled curve with $D_i \propto C^2$.

The Zn profile in Figure 4.7 for a 5 minute diffusion clearly presents the case of diffusion under non-equilibrium conditions. Here, Zn atoms diffuse in the GaAsSb lattice but the diffusion does not take place long enough for reaction (4.23) to reach equilibrium. Much lower activation of 42 % is observed in this case.

In all the profiles shown above, Zn concentration away from the surface follows the error function complementary curve, which is the characteristic of Fickian diffusion. The concentration-independent diffusivity, D_s , obtained for the three cases are also quite close to each other. It is possible that the diffusing species is $[\text{Zn}_{\text{Ga}}^-]$, which diffuses via a Ga vacancy. However, this seems unlikely because the diffusivity

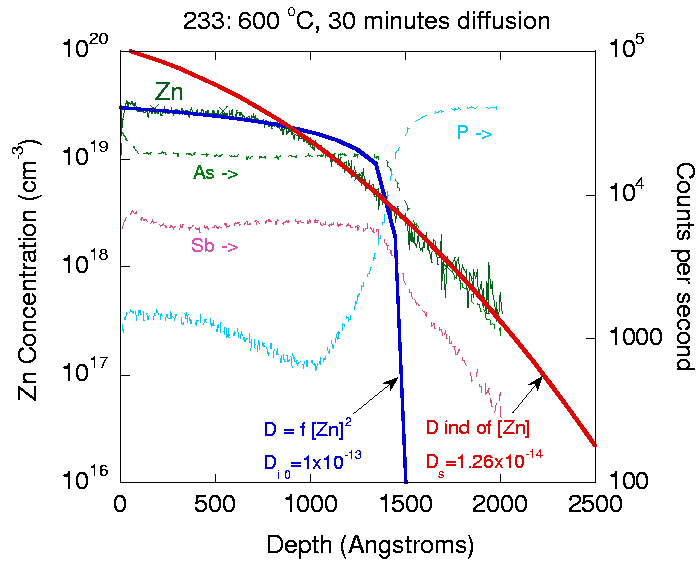


Figure 4.5. Modeled and experimental Zn distribution profiles in test structure 233 for a 600 °C, 30 minute diffusion.

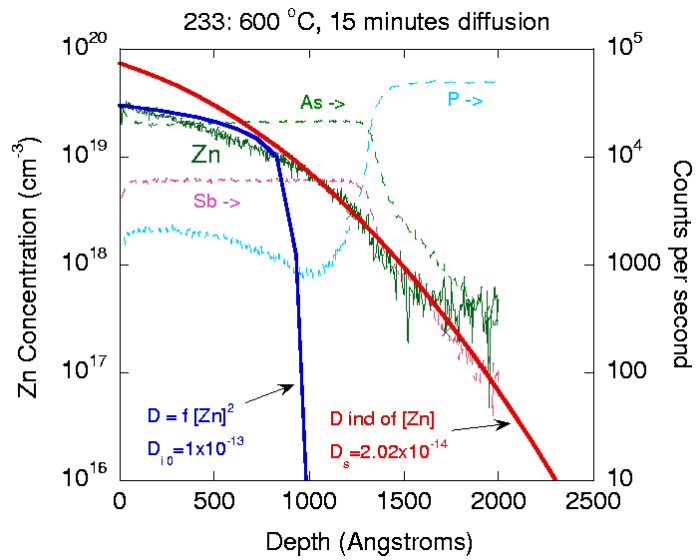


Figure 4.6. Modeled and experimental Zn distribution profiles in test structure 233 for a 600 °C, 15 minute diffusion.

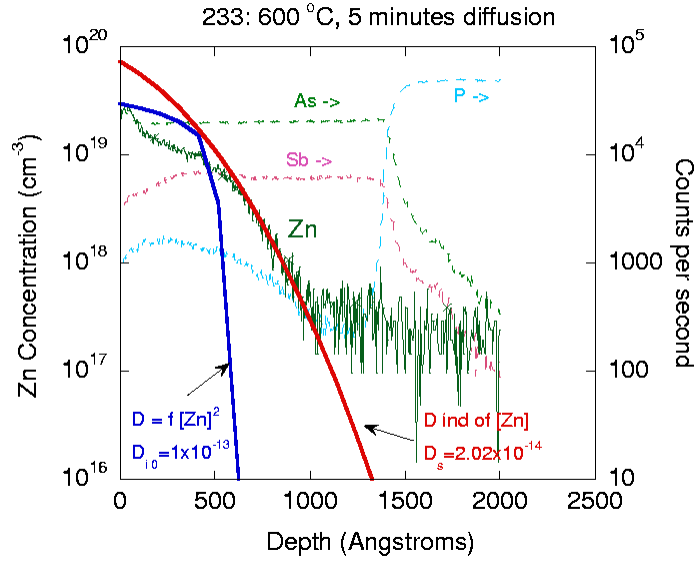


Figure 4.7. Modeled and experimental Zn distribution profiles in test structure 233 for a 600 °C, 5 minute diffusion.

of $1 - 2 \times 10^{-14} \text{ cm}^2/\text{s}$ appears to be very high for relatively immobile Zn_{Ga} . The diffusing species is more likely to be a complex of Zn_{Ga} and a defect, and the complex diffuses due to the concentration gradient along the lattice with a diffusivity that is between the interstitial Zn diffusivity and substitutional Zn diffusivity.

Based on the arguments presented above, the following diffusion mechanism for test structure 233 is proposed:

Close to the surface, there is high concentration of Zn atoms and not all Zn atoms get substitutionally incorporated in the GaAsSb lattice. Some of the Zn exists as interstitials, which have higher diffusivity, and diffuse inside the lattice until they combine with a Ga vacancy or form a complex with the surrounding defects. The Zn complexes are more mobile than substitutional Zn and diffuse inside due to the concentration gradient.

This mechanism also accounts for the increase in Zn diffusion when the back-

ground doping increases (and hence the hole concentration). To compensate for this increase, reaction (4.23) shifts towards left producing more interstitial Zn. Interstitial Zn has a higher diffusivity and Zn diffusion is enhanced, as is observed from SIMS and Hall-effect data.

CHAPTER 5

CONCLUSION

Zn diffusion from spin-on glass dopant sources in p-type GaAs_{0.51}Sb_{0.49} epitaxially grown on InP was investigated. It is observed that Zn starts to diffuse into GaAsSb at temperatures as low as 350 °C, however, the Zn atoms remain largely electrically inactive at temperatures below 500 °C. The threshold temperature for Zn activation in GaAsSb is found to be between 500–550 °C. At 600 °C, Zn activation of 80–100 % was observed in all samples. Good electronic transport properties were observed in Zn doped GaAsSb: hole concentration as high as $2.5 \times 10^{19} \text{ cm}^{-3}$, sheet resistance as low as 358 Ω/sq . and a mobility of 35 cm^2/Vs was observed in 2000 Å thick GaAs_{0.51}Sb_{0.49} with as-grown doping of $9.65 \times 10^{17} \text{ cm}^{-3}$. The effect of increasing the background doping on Zn diffusion was also investigated. Zn diffusion was found to increase when diffusions were performed in GaAsSb layers with higher as-grown doping levels.

Zn appears to diffuse differently in GaAs_{0.51}Sb_{0.49} than in GaAs and GaSb. Zn profiles in GaAs_{0.51}Sb_{0.49} exhibit a gradual diffusion front in contrast to a very steep diffusion front observed in both GaAs and GaSb. Zn diffuses by interstitial-substitutional mechanism in the region close to the surface with diffusivity, D_{i0} , of $1 \times 10^{-13} \text{ cm}^2/\text{s}$ at 600 °C for interstitial Zn. Away from the surface, a substitutional mechanism explains the Zn diffusion and diffusivity of $1\text{--}2 \times 10^{-14} \text{ cm}^2/\text{s}$ at 600 °C is extracted from Zn profiles in the bulk.

By utilizing the spin-on dopant technique, near-ideal box shaped Zn profiles that are confined to the 400 Å thick GaAs_{0.51}Sb_{0.49} base layer of InP/GaAsSb/InP DHBT structure, with total Zn concentration in excess of $2 \times 10^{19} \text{ cm}^{-3}$, have been demonstrated. However, the Zn atoms cause the sheet resistance of the GaAsSb layer to increase further rendering the Zn diffusion from spin-on dopant technique unsuitable for application in HBTs. This study concludes that post-growth selective doping of the extrinsic base region InP/GaAsSb/InP DHBTs using spin-on dopant technique for achieving higher f_{MAX} , although attractive in concept, could not be demonstrated in practice.

BIBLIOGRAPHY

- [1] "40 Gbps link enjoys success in real-world trial." www.compoundsemiconductor.net, 16 June 2004.
- [2] M. J. W. Rodwell, M. Urteaga, Y. Betser, T. Mathew, P. Krishnan, D. Scott, S. Jaganathan, D. Mensa, J. Guthrie, R. Pallela, Q. Lee, B. Agarwal, U. Bhattacharya, and S. Long, "Scaling of InGaAs/InAlAs HBTs for high speed mixed-signal and mm-wave ICs," *International Journal of High Speed Electronics and Systems*, vol. 11, pp. 159-215, 2001.
- [3] K. Yang, J. C. Cowles, J. R. East, and G. I. Haddad, "Theoretical and Experimental DC Characterization of InGaAs-Based Abrupt Emitter HBT's," *IEEE Transactions on Electron Devices*, vol. 42, pp. 1047-1058, 1995.
- [4] W. Hafez, J. W. Lai, and M. Feng, "Vertical Scaling of 0.25- μ m Emitter InP/InGaAs Single Heterojunction Bipolar Transistors With f_T of 452 GHz," *IEEE Electron Device Letters*, vol. 24, pp. 436-438, 2003.
- [5] C. R. Bolognesi, N. Matine, M. W. Dvorak, P. Yeo, X. G. Xu, and S. P. Watkins, "InP/GaAsSb/InP Double HBTs: A New Alternative for InP-Based DHBTs," *IEEE Transactions on Electron Devices*, vol. 48, pp. 2631-2639, 2001.
- [6] C. R. Bolognesi, M. W. Dvorak, N. Matine, O. J. Pitts, and S. P. Watkins, "Ultrahigh Performance Staggered Lineup ("Type-II") InP/GaAsSb/InP NpN Double Heterojunction Bipolar Transistors," *Japanese Journal of Applied Physics*, vol. 41, pp. 1131-1135, 2002.
- [7] B. T. McDermott, E. R. Gertner, S. Pittman, C. W. Seabury, and M. F. Chang, "Growth and doping of GaAsSb via metalorganic chemical vapor deposition for InP heterojunction bipolar transistor," *Applied Physics Letters*, vol. 68, pp. 1386-1388, 1996.
- [8] D. Sawdai, X. Zhang, D. Pavlidis, and P. Bhattacharya, "Performance Optimization of PNP InAlAs/InGaAs HBTs," *16th Biennial IEEE/Cornell University Conference on Advanced Concepts in High-Speed Semiconductor Devices and Circuits, August 1997*. <http://www.eecs.umich.edu/dp-group/HBT/cornell97/>
- [9] S. Sze, "Physics of Semiconductor Devices," (2nd Edition, Wiley, New York 1981), pp. 144-145.
- [10] Emulsitone Company, 19 Leslie Court, Whippany, N.J. 07981, Phone: 973-386-0053, www.emulsitone.com.

- [11] D.Mathiot, A.Lachiq, A.Slaoui, S.Noel, J.C.Muller, C.Dubois, "Phosphorous diffusion from spin-on doped glass (SOD) source during rapid thermal annealing," *Material Science in Semiconductor Processing*, vol. 1, pp. 231-236, 1998.
- [12] L. J. van der Pauw, "A Method of Measuring Specific Resistivity and Hall Effect of Discs of Arbitrary Shapes," *Philips Res. Repts.*, vol. 13, pp. 1-9, 1958.
- [13] "Hall Effect Measurements," <http://www.eeel.nist.gov/812/hall.html>
- [14] Charles Evans Associates, 810 Kifer Sunnyvale CA 94086-5203, Phone: 408-530-3500, www.eaglabs.com.
- [15] A. V. Kamanin, Y. A. Kudryavtsev, and N. M. Shmidt, "Threshold Character of Zn Diffusion into InP," *Diffusion Mechanisms in Crystalline Materials. Symposium*, pp. 413-416, 1998.
- [16] B. T. McDermott, E. R. Gertner, S. Pittman, C. W. Seabury, and M. F. Chang, "Growth and doping of GaAsSb via metalorganic chemical vapor deposition for InP heterojunction bipolar transistors," *Applied Physics Letters*, vol. 68, pp. 1386-1388, 1996.
- [17] D. Yu, K. Lee, B. Kim, D. Ontiveros, K. Vargason, J. M. Kuo, and Y. C. Kao, "Ultra High-Speed InP-InGaAs SHBTs With f_{MAX} of 478 GHz," *IEEE Electron Device Letters*, vol. 24, pp. 384-386, 2003.
- [18] M. W. Dvorak, N. Matine, C. R. Bolognesi, X. G. Xu, and S. P. Watkins, "Design and performance of InP/GaAsSb/InP double heterojunction bipolar transistors," *Journal of Vacuum Science and Technology A: Vacuum, Surfaces, and Films*, vol. 18, pp. 761-764, 2000.
- [19] B. Tuck, "Mechanisms of atomic diffusion in the III-V semiconductors," *Journal of Physics D: Applied Physics*, vol. 18, pp. 557-584, 1985.
- [20] N. Arnold, R. Schmitt, and K. Heime, "Diffusion in III-V semiconductors from spin-on film sources," *Journal of Physics D: Applied Physics*, vol. 17, pp. 443-474, 1984.
- [21] R. L. Longini, "Rapid Zinc Diffusion in Gallium Arsenide," *Solid State Electronics*, vol. 5, pp. 127-130, 1962.
- [22] L. R. Weisberg, and J. Blanc, "Diffusion with Interstitial-Substitutional Equilibrium. Zinc in GaAs," *Physical Review*, vol. 131, pp. 1548-1552, 1963.
- [23] B. Tuck, M. A. Kadhim, "Anomalous diffusion profiles of zinc in GaAs," *Journal of Material Science*, vol. 7, pp. 585, 1972.
- [24] U. Gosele, and F. Morehead, "Diffusion of zinc in gallium arsenide," *Journal of Applied Physics*, vol. 52, pp. 4617-4619, 1981.
- [25] A. H. van Ommen, "Examination of models for Zn diffusion in GaAs," *Journal of Applied Physics*, vol. 54, pp. 5055-5058, 1983.

- [26] A. S. Kyuregyan, and V. M. Stuchechnikov, "Diffusion of Zinc in Gallium Antimonide," *Soviet Physics - Semiconductors*, vol. 4, pp. 1365, 1971.
- [27] G. J. Conibeer, A. F. W. Willoughby, C. M. Hardingham, and V. K. M. Sharma, "Zinc Diffusion in Tellurium Doped Gallium Antimonide," *Journal of Electronic Materials*, vol. 25, pp. 1108-1112 , 1998.
- [28] S. P. Nicols, H. Bracht, M. Benamara, Z. Liliental-Weber, E. E. Haller, "Mechanism of zinc diffusion in gallium antimonide," *Physica B*, 3-0-310, pp. 854-857, 2001.
- [29] S. Dakshinamurthy, S. Shetty, I. Bhat, C. Hitchcock, R. Gutmann, G. Charache, and M. Freeman, "Fabrication and Characterization of GaSb Based Thermophotovoltaic Cells Using Zn Diffusion from a Doped Spin-On Glass Source," *Journal of Electronic Materials*, vol. 28, pp. 355-359, 1999.